Relation-Oriented: Toward Causal Knowledge-Aligned AGI

Anonymous authors
Paper under double-blind review

Abstract

The current relationship modeling paradigm, grounded in the observational i.i.d assumption, fundamentally misaligns with our causal knowledge understanding due to two key oversights: 1) the unobservable relations, which lead to undetectable hierarchical levels of knowledge, driving the need for model generalizability; 2) the cognitive relative timings, which crucially support our structural knowledge comprehension, resulting in inherent biases within the present *Observation-Oriented* paradigm. Adopting a novel *Relation-Oriented* perspective, this paper proposes a new framework to unify the various confusions surrounding causality learning, ranging from traditional causal inference to modern language models.

Also, relation-indexed representation learning (RIRL) is raised as a baseline implementation method of the proposed new paradigm, alongside comprehensive experiments demonstrating its efficacy in autonomously identifying dynamical effects in relationship learning.

1 Introduction

The concept of Artificial General Intelligence (AGI) has prompted extensive discussions over the years Newell (2007), with the central target toward facilitating human-like causal reasoning and comprehension in AI systems Marcus (2020). In recent years, the large language models (LLMs) have risen as notable achievements in language-understanding tasks and accordingly evoked debates about whether LLMs have edged us closer to realizing AGI Rylan (2023). Some studies point to their shortcomings in truly comprehending causality Pavlick (2023), while others argue in favor of LLMs' ability to represent complex spatial and temporal features Wes (2023). Notably, the use of meta-learning in language models has shown potential in achieving human-like generalization capabilities, at least to a certain extent Lake (2023).

These debates are anchored in an underlying inquiry: What underpins the distinction between two types of generalization? One is how humans generalize learned causal knowledge to diverse scenarios, and another is how AI systems generalize associative knowledge among texts and images.

It appears that classical causal inference has offered a clear delineation between causality and mere correlations or associations Pearl et al. (2000); Peters et al. (2017). Moreover, it has established a robust theoretical groundwork for representing causality in computational models - Building on which, widely utilized causal learning techniques have yielded significant contributions to the accumulation of causal knowledge in various fields Wood (2015); Vuković (2022); Ombadi (2020). It is thus logical to incorporate existing causal knowledge, often represented as causal DAGs (Directed Acyclic Graphs), into AI model architectures Marwala (2015); Lachapelle et al. (2019). While this integration has greatly enhanced learning efficiency, it has not yet achieved the level of generalizability that constitutes a success Luo (2020); Ma (2018).

This likely circles us back to the initial question, as causal inference cannot directly bridge the gap between human-like causal reasoning and current AI systems. However, it does offer a different perspective: How would humans conduct causal reasoning based solely on DAGs? A task that evidently challenges AI.

Even within the realm of causal inference, the process of converting DAGs into operational causal models is rigorous Elwert (2013). Tailored adjustments and interpretations are often required, reliant on human discernment across varied applications Sanchez (2022); Crown (2019). Key challenges include establishing fundamental causal assumptions Sobel (1996), addressing confounding effects Greenland (1999), ensuring model interpretability Pearl et al. (2000), etc. These achievements constitute the cornerstone of the value provided by causal inference methodologies. It stands to reason that the answer to this fundamental question may be gleaned from examining the challenges that causal inference has faced and partially overcome.

From an applicational standpoint, Scholkopf (2021) have synthesized the development of current causal models, underscoring the pivotal role of realizing "causal representations" to achieve the generalizability of AI-based causal models across different "levels of knowledge" learning. They propose the potential need for a "new learning paradigm" - an idea we find both logical and thought-provoking. Our current models, ranging from causal to AI, are chiefly based on the assumption of independent and identically distributed (i.i.d.) observations, a paradigm that may be hindering their ability to autonomously realize generalizable causal reasoning. On the other hand, Zhang (2012) points out the "identifiability difficulty" when facing nonlinear effects, an inherent obstacle under the i.i.d observational effect setting.

For clarity, we designate the prevailing paradigm as ***Observation-Oriented*** modeling. In this study, we propose a novel paradigm, termed ***Relation-Oriented*** modeling, inspired by the relation-indexing nature of human cognition processes Pitt (2022). Through this new lens, we seek to pinpoint the intrinsic limitations of the existing paradigm. Accordingly, to validate the proposed new paradigm, it must shed light on the array of questions that have emerged from the outset. To encapsulate these queries:

- ❖ *Firstly*, causal inference challenges such as confounding effects, dependency on causal assumptions, and interpretative complexities call for a foundational explanation.
- ❖ *Secondly*, To integrate causal reasoning within AI models, we need a nuanced understanding of "levels of knowledge," the essential role of causal representation, its relevance to the difficulty of identifying nonlinear effects, and potential resolutions to these issues.
- ❖ *Thirdly*, in the context of Large Language Models (LLMs), we must discern the distinction between the "spatial and temporal" conceptions in language versus causality comprehension, and critically assess what meta-learning has accomplished in terms of generalizability.

While these questions might seem disparate, they are intrinsically linked to the fundamental requirement by the *Observation-Oriented* paradigm: it necessitates the prior specification of observable entities (including temporal events). In solely observational learning tasks (like image recognition), these entities serve as the modeling target. In causal relationship learning, they are priorly identified as causes and effects, with their interrelation acting as the primary learning objective.

This fundamental requirement introduces two ***primary limitations*** in modeling: 1) the inability to account for unobservable relational knowledge, which leads to undetectable hierarchical levels in modeling, and 2) the obligation to assign timestamps to events, potentially causing the overlook of relative timings underpinning structuralized dynamics in our relational knowledge, and essentially introducing inherent biases.

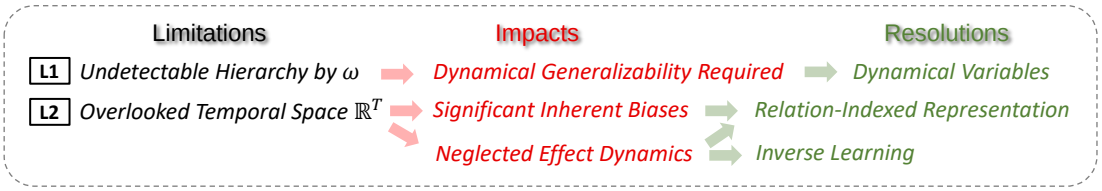

Figure 1: Overview of the *Observation-Oriented* paradigm's primary limitations (labeled as L1 and L2), featuring the concept of hidden relation ω (see section 1.2) and the temporal space $\mathbb{R}^T$ with relative timing axes (discussed in section 2.1).

This paper consists of four principal parts:

1. the Introduction, which sets the foundation for the proposed *Relation-Oriented* perspective in section 1.1, and analyze the roles of unobservable relational knowledge in modeling, using an illustrative example to explain its resulting undetectable hierarchy in section 1.2 (i.e., the limitation L1).
2. Chapter I, including Sections 2 through 4, establishes the *Relation-Oriented* framework to decompose relationship modeling from a more precise perspective, and through this framework, examines the fundamental impacts of the outlined limitations, and addresses the queries listed above.
3. Chapter II, from Sections 5 to 7, introduces *Relation-Indexed Representation Learning* (RIRL) as a baseline realization method of the *Relation-Oriented* paradigm and evaluates the efficacy of relation-indexed autonomous effect identification.
4. the Conclusion in Section 8 summarizes the insights and findings of this study.

1.1 Relation-Oriented Perspective

Typically, experiments with n trials produce instances $x^n = (x_1, \ldots, x_n)$ from sequential random variables $X^n = (X_1, \ldots, X_n)$, which are usually assumed to be independent and identically distributed (i.i.d.). When these variables evolve over time, n is often replaced by the timestamp t to get temporal sequence $X^t = (X_1, \ldots, X_t)$, maintaining the i.i.d. assumption, and the relationship function is in shape $Y = f(X^t; \theta)$.

In our research, we abandon the i.i.d. assumption for $\{X_i \mid i = 1, \ldots, t\}$ over the temporal dimension $\mathbf{t}$, instead treat their sequence X^t as a single entity, denoted by variable $\mathcal{X} \in \mathbb{R}^{d+1}$, with d representing the observational dimension of each instance X_i. For clarity, we use $X \in \mathbb{R}^d$ to represent a solely observational variable, and let $\mathcal{X} = \langle X, \mathbf{t} \rangle \in \mathbb{R}^{d+1}$ derived by incorporating the $\mathbf{t}$-dimension to encompass features across both observational and temporal dimensions. It is worth noting that variables such as $\mathcal{X}$ are conventionally referred to as spatial-temporal Andrienko (2003). However, in this context, "spatial" is broadly interpreted to mean "observational" and is not restricted to physical spatial data, such as geographic coordinates.

Consider the functional relationship $\mathcal{Y} = f(\mathcal{X}; \theta)$, where $\mathcal{Y} = \langle Y, \tau \rangle \in \mathbb{R}^{b+1}$ with τ representing the temporal evolution of $Y \in \mathbb{R}^b$. We employ the Fisher Information $\mathcal{I}_{\mathcal{X}}(\theta)$ Ly et al. (2017) of $\mathcal{X}$ about θ, to define the component of $\mathcal{Y}$ (signified as $\hat{\mathcal{Y}}$) that is sufficiently identified by indexing through θ:

Definition 1. the *Relation-Indexed Representation* $\hat{\mathcal{Y}}_\theta$ in Relationship Modeling.

Let the ***relation*** θ adequately represents the influence of $\mathcal{X}$ on $\mathcal{Y}$, denoted as $\mathcal{X} \xrightarrow{\theta} \mathcal{Y}$, then $\hat{\mathcal{Y}}_\theta = f(\mathcal{X}; \theta)$ represents the *sufficient* component of $\mathcal{Y}$ about θ, which is, $\mathcal{I}_{\hat{\mathcal{Y}}_\theta}(\theta) = \max\ \mathcal{I}_{\hat{\mathcal{Y}}}(\theta) = \mathcal{I}_{\mathcal{X}}(\theta)$.

Consequently, $\hat{\mathcal{Y}}_\theta$ encapsulates the information within $\mathcal{Y}$ that is entirely derived from $\mathcal{X}$, thus defined as the *relation-indexed representation*. Accordingly, the remaining component of $\mathcal{Y}$, expressed as $\mathcal{Y} - \hat{\mathcal{Y}}_\theta$, does not depend on θ. The *Relation-Oriented* perspective focuses on building models by concentrating on θ.

The notation "$\rightarrow$" typically denotes causality, although a directional relationship does not always imply causality in logic. Nonetheless, for clarity, we will adopt terminology consistent with causal inference: for relationship $\mathcal{X} \xrightarrow{\theta} \mathcal{Y}$, we refer to $\mathcal{X}$ as the *cause* and $\mathcal{Y}$ as the *effect*, with a *relation* θ connecting them. Accordingly, $\hat{\mathcal{Y}}_\theta$ represents the component of effect determined by the cause, aligned with the "causal representation" concept Scholkopf (2021). It is important to distinguish that both *causality* and *correlation* are types of relationships (their difference will be discussed later), while *association* indicates only statistical dependency without an informative θ.

Remark 1. Given $\mathcal{X} \xrightarrow{\theta} \mathcal{Y}$ with ***observables*** $\mathcal{X}$ and $\mathcal{Y}$, the relationship model $\mathcal{Y} = f(\mathcal{X}; \theta)$ becomes *informative* due to the ***unobservable*** θ.

The principle outlined in Remark 1 has its origins in the concept of Common Cause Dawid (1979); Scholkopf (2021), suggesting that any nontrivial (i.e., informative) conditional independence between two observables requires a third, mutual cause (i.e., the unobservable "relation" in our context). It means that an informative θ differentiates a causal relationship $\mathcal{X} \xrightarrow{\theta} \mathcal{Y}$ from a mere statistical dependency, expressed as $\mathbf{P}(\mathcal{Y} \mid \mathcal{X})$.

Here, $\mathcal{X}$ and $\mathcal{Y}$ can be either solely observational entities, equal to X and Y (e.g., images, spatial coordinates of a quadrotor, etc.), or observational-temporal entities (e.g., trends of stocks, a quadrotor's trajectory, etc.). Regardless of their characterization, the primary goal of utilizing the function $\mathcal{Y} = f(\mathcal{X}; \theta)$ is to encapsulate the unobservable relational knowledge represented by θ, rather than merely direct observational associations between $\mathcal{X}$ and $\mathcal{Y}$, denoted by $(\mathcal{X}, \mathcal{Y})$.

To clarify the concept of informative θ, let's consider a simple example. In the relationship "Bob (represented as X) has a son named Jim (represented as Y)", the father-son relation information $\mathcal{I}(\theta)$ between them is evident to human cognition but unobservable to AI provided sufficiently observed social activities. Also, θ can be seen as the common cause of X and Y that makes their connection unique, rather than any random pairing of "Bob" and "Jim". Through the observational data, AI might deduce a particular interactive pattern between (X, Y), but cannot internalize the unobservable information $\mathcal{I}(\theta)$ between them.

Drawing on the symbolization provided in Definition 1, a comprehensive *Relation-Oriented* framework is introduced in Section 2, offering more complete insights into the modeling of causal relationships.

1.2 Unobservable Relational Knowledge

Unobservable knowledge may not directly serve as the learning objective relation θ, but it can still be relative to and profoundly impact the modeling process. We elucidate this with the following example: It is notable that on social media, AI-created personas can have realistic faces but seldom showcase hands. This is because AI for visual tasks struggles with the intricate structure of hands, instead treating them as arbitrary assortments of finger-like items. Figure 2(a) provides AI-created hands with faithful color but unrealistic shapes, while humans can effortlessly discern hand gestures from the grayscale sketches in (b).

Humans intuitively employ informative relations as the ***indices***, guiding us to specific mental representations Pitt (2022). As illustrated in Figure 2(b), our cognition operates hierarchically, progressing through a series of relations, denoted as $\theta = (\theta_i, \theta_{ii}, \theta_{iii})$. Each higher-level understanding builds upon conclusions drawn at preceding levels. Specifically, Level **I** identifies individual fingers; Level **II** distinguishes gestures based on the positions of the identified fingers, incorporating additional information from our understanding of how fingers are arranged to constitute a hand, denoted by ω_i; and Level **III** grasps the meanings of these gestures from memory, given additional information ω_{ii} from knowledge.

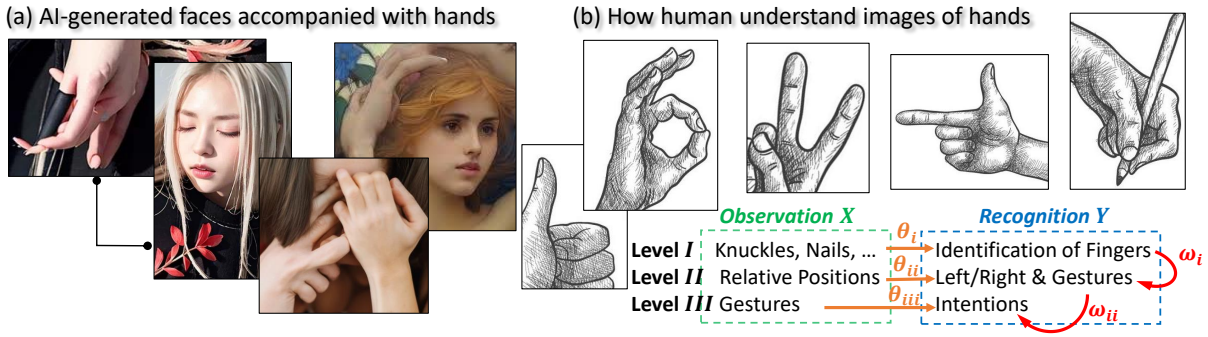

Figure 2: Unobservable relations $\theta = (\theta_i, \theta_{ii}, \theta_{iii})$ and $\omega = (\omega_i, \omega_{ii})$. AI can generate reasonable faces but treat hands as arbitrary mixtures of fingers. In contrast, human cognition processes observations hierarchically to avoid this mess, by indexing through a series of relations $\theta = (\theta_i, \theta_{ii}, \theta_{iii})$.

Typically, these visual association learning tasks do not aim to model relations, neither θ nor $\omega = (\omega_i, \omega_{ii})$. Instead, they focus on capturing observational distributions (pertaining solely to X). Without relation-indexing through θ, the AI system may not distinguish entities across different levels but can only capture their dependencies (e.g., $\mathbf{P}(X_{II} \mid X_I)$) without deeper, informative insights into ω.

However, for such solely observational learning, the hidden information of ω may not be essential. If entities across levels are observationally distinct and non-overlapping, AI can accurately differentiate them. For instance, AI can generate convincing faces because the appearance of eyes strongly indicates facial angle, removing the need to distinguish "eyes" (X_{II}) from "faces" (X_I). Additionally, based on fully-captured levels, AI can inversely uncover the hidden ω using methods such as reinforcement learning Sutton (2018); Arora (2021) - In this case, approvals of generated five-fingered hands may lead AI to identify fingers autonomously.

Definition 2. *Hidden Relation* ω and its resulting *Undetectable Hierarchy*.
Different from the ***indexing*** *relation* θ, the ***hidden*** *relation* ω can constitute *undetectable hierarchical levels* of knowledge, requiring model *generalizable* to be effective across.

A *generalizable* model enables the learned lower-level relationships to be reusable for higher-level learning tasks Scholkopf (2021), which mirrors our inherent capability to generalize knowledge in cognition. For example, our ability to identify fingers can be applied regardless of the types of medium, like images, photos, or videos. Conversely, generalizability also denotes the capacity to *individualize* from higher to lower levels, accommodating different ω values.

The illustration in Figure 2 highlights the distinct roles of unobservable relations (θ and ω) in modeling. Our central concern, however, is the modeling of relationships with θ as the primary ***objective*** *relation* for learning. In this context, ω stratifies the unobservable θ into hierarchical levels, culminating in a completely imperceptible joint distribution of (θ, ω), which precludes methods like inverse reinforcement learning.

For instance, consider the relation θ, through which family incomes X influence grocery shopping frequencies Y. Here, the cultural background, symbolized as ω, emerges as an important factor, such that an effective model $Y = f(X; \theta)$ has to be individualizable, i.e., conditioned on a specific country (represented by a particular ω value) to ensure practical utility. On the opposite, a generalization would imply $\omega = \varnothing$.

For the sake of clarity, hereafter in this paper, unless explicitly stated otherwise, the hidden relation ω represents two hierarchical modeling levels: the generalized level $X_o \xrightarrow{\theta_o} Y_o$ with θ_o implying $\omega = \varnothing$, and the individualized level $X_\omega \xrightarrow{\theta_\omega} Y_\omega$ given θ_o with a specific ω value, collectively notated as $(\theta, \omega) = \begin{pmatrix} \theta_o \\ \theta_\omega \end{pmatrix}$.

Chapter I: Limitations of Current Observation-Oriented Paradigm

The prevalent *Observation-Oriented* modeling paradigm inherently misaligns with the relation-centric human comprehension Pitt (2022). This misalignment may not have been critical in the past. In traditional causal inference, challenges could be addressed through intended adjustments due to the limited scale of questions. Nonetheless, with the advancements in AI-based large models, the consequences of this misalignment have become increasingly significant across various applications.

Section 2 establishes a *Relation-Oriented* dimensionality framework to symbolize causal relationship models; through which, we recognize the critical role of relative timings (highlighted as limitation L2), and explore the essence of generalizability for a relationship model comprising structuralized dynamics. Subsequently, Section 3 delves into the critical implications of overlooked effect dynamics (the secondary impact of L2), and accordingly reevaluates the traditional causal inference challenges within the new framework. Lastly, Section 4 elucidates the inherent biases that *Observation-Oriented* causal models introduce into structural causal relationship learning (the primary impact of L2).

2 Relation-Oriented Dimensionality Framework

In the fervent debates surrounding AGI, a pivotal question persists: Can conceptualized symbols and AI systems grounded in symbolism truly represent a human-like comprehension for empirical inquiries Newell (2007); Pavlick (2023). We suggest that the essence lies in enabling informative symbolization. Within our cognitive framework, elements that are abstractly meaningful can be represented as unobservable variables. By directing the learning objective towards extracting these elements from observable data, the symbolized computation within the model remains informative. Such captured relational information has the potential to mirror our cognitive processes of logical deduction.

Given Definitions 1 and 2, symbolizing a directional relationship necessitates two types of variables: the unobservable (θ, ω), and the observables $\{\mathcal{X}, \mathcal{Y}\}$. As defined, $\mathcal{X}$ and $\mathcal{Y}$ encompass both observational features and temporal features. Correspondingly, we introduce a conventional conception of *hyper-dimension* to incorporate the unobservable features (θ, ω), establishing a framework as depicted in Figure 3, to represent relationships as joint distributions across three distinct types of dimensions. For clarity, "feature" refers to the potential variable fully representing a certain distribution of interest.

Figure 3 aims to represent our cognitive space, where the relational comprehension of causal knowledge is stored. The hyper-dimensional space $\mathbb{R}^H$ is constructed by aggregating all unobservable relations in our knowledge, such as $(\theta, \omega) \in \mathbb{R}^H$. Conversely, the observational-temporal joint space, comprising $\mathbb{R}^O \cup \mathbb{R}^T$, is referred to as the "observable space." Within both $\mathbb{R}^O$ and $\mathbb{R}^T$, temporal dimensions denote the evolution of timing, and the nonlinear distributions in these dimensions indicate temporal dynamical features. The distinction between *dynamical* and *static* features will be elaborated upon in section 2.2.

In time series data matrices, the attribute (typically a column) recording the observed timestamps usually indicates the *absolute* timing of reality, denoted by $\mathbf{t}$. Nonetheless, beyond the observational $\mathbf{t}$ dimension, our cognitive space inherently comprises abstract *relative* timings Wulf (1994) where structural knowledge resides. Therefore, we use a distinct "temporal space" $\mathbb{R}^T$, separate from the observational space $\mathbb{R}^O$, to integrate knowledge-aligned temporal features, treating T relative timings as T dimensions.

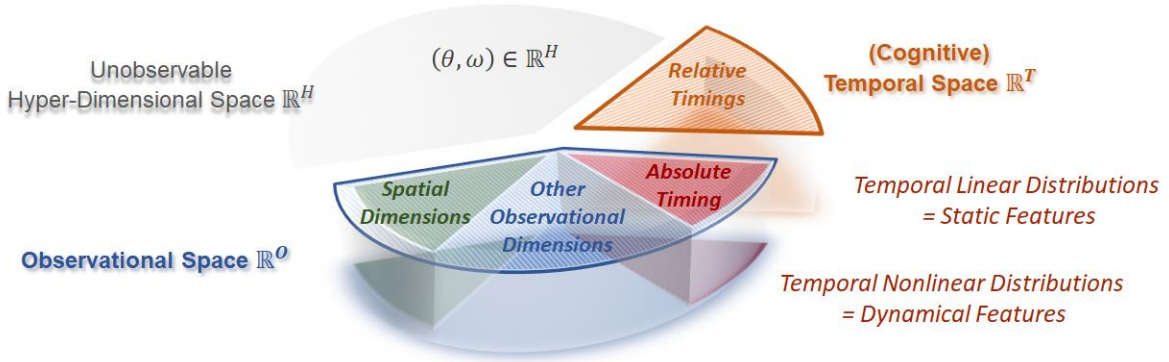

Figure 3: *Relation-Oriented* Dimensionality Framework: splitting the knowledge-storing cognitive space by their accommodated features, where $\{\mathcal{X}, \mathcal{Y}\} \in \mathbb{R}^O$, $\{X^t, Y^t\} \in \mathbb{R}^{O-1}$, and (θ, ω) lies in unobservable $\mathbb{R}^H$.

Definition 3. The *Relationship Symbolization* within the proposed Dimensionality Framework.
For the relationship $\mathcal{X} \xrightarrow{\vartheta} \mathcal{Y}$, where $\{\mathcal{X}, \mathcal{Y}\} \in \mathbb{R}^O$ and $\vartheta \in \mathbb{R}^T \cup \mathbb{R}^H$. The ***structuralized*** *relation* ϑ can be decomposed as:

$$\vartheta = \overrightarrow{\theta^1, \ldots, \theta^T} = \overrightarrow{\theta^i} \text{ with } i = 1, \ldots, T \text{ and } \theta^i \in \mathbb{R}^H. \text{ Accordingly,}$$

$$(\vartheta, \omega) = \begin{pmatrix} \vartheta_o \\ \vartheta_\omega \end{pmatrix} = \begin{pmatrix} \theta_o^1 & \ldots & \theta_o^T \\ \theta_\omega^1 & \ldots & \theta_\omega^T \end{pmatrix} = \begin{pmatrix} \overrightarrow{\theta_o^i} \\ \overrightarrow{\theta_\omega^i} \end{pmatrix} \text{ with } i = 1, \ldots, T \text{ and } \{\omega, \theta_o^i, \theta_\omega^i\} \in \mathbb{R}^H.$$

2.1 Absolute Timing vs. Relative Timings

From a modeling perspective, absolute timestamps in datasets are not readily distinguishable from other observational attributes. Thus, we consider these observed timestamps as a single *absolute timing* dimension within the observational space $\mathbb{R}^O$. Within $\mathbb{R}^O$, both $\mathcal{X}$ and $\mathcal{Y}$ are invariably observed as data sequences X^t and Y^t, each consistently marked along the absolute timing $\mathbf{t}$.

Whereas, when $\{\mathcal{X}, \mathcal{Y}\}$ are considered alongside ϑ within the joint space $\mathbb{R}^O \cup \mathbb{R}^T$, it suggests that ϑ could span multiple *relative timing* dimensions in $\mathbb{R}^T$, which serve as distinct *timelines* in our cognitive framework to house those structuralized relational knowledge Shea (2001). Accordingly, as the effect of a structuralized ϑ, observational-temporal features within $\mathcal{Y}$ can be decomposed into T elements $\mathcal{Y} = (\mathcal{Y}_1, \ldots, \mathcal{Y}_T)$ with each reside one of the timelines; they may be interacted, forming a structural relationship within $\mathbb{R}^O \cup \mathbb{R}^T$. Although the underlying structure is not directly observable, collectively assuming all featured dynamical events confined within $\mathbb{R}^O$ along the single absolute timing $\mathbf{t}$ can be problematic.

For instance, all patients' vital signs are recorded daily in the hospital, marked with the *absolute* chronological timestamps. Yet, to access a medical intervention, a uniform series of specific post-medication events must be selected - say, from one day after medication to the 30th day following it - to establish a timeline from 1 to 30 representing this *relative* timing, regardless of the varying *absolute* timestamps of the records. Furthermore, when two vital signs evolve along two distinct relative timings, assigning absolute timestamps for their identification will risk overlooking their unique dynamic evolutions.

Consequently, when considering an observational-temporal effect variable $\mathcal{Y}$ that includes a timing dimension τ, it is not necessary for τ to be strictly absolute or relative; it may even represent multiple underlying timing dimensions depending on the specific context.

Remark 2. The *temporal dimension* in a causal relationship is not limited to a single dimension but can include multiple timing axes (i.e., timelines) to form a multi-dimensional *temporal space*.

In modeling, the "temporal dimension" is often simplistically equated with a single **t** axis comprising the observed timestamps from data, as seen from "spatial-temporal" analysis in conventional studies Alkon (1988); Turner (1990); Andrienko (2003), to recent advancements in language models Wes (2023). However, this perspective does not align with our cognitive understanding of "time", which is more intricate and forms the basis for constructing our causal knowledge Coulson (2009).

To provide an intuitive insight into the implications of neglecting relative timings in modeling, let's consider an analogy: Imagine ants dwelling on a floor's two-dimensional plane. To predict risks, the scientists among them create two-dimensional models and instinctively adopt the nearest tree as a height reference. They noticed an increase in disruptions at the tree's mid-level, which indeed correlates to the children's heights, given their curiosity. However, without understanding humans as three-dimensional beings, the interpretation from ants is limited at the tree's mid-level. One day, after relocating to another tree with a different height, the ants found the mid-level no longer presenting a high risk, making their model ineffective. They may conclude that human behaviors are too complex, highlighting the model generalizability issue.

As three-dimensional beings, we inherently lack the capacity to fully integrate the fourth dimension - time - into visual perception. Instead, we conceptualize "space" in three dimensions to incorporate features of the temporal dimension along a timeline, analogous to our "tree". Similarly, just as ants do not need to fully comprehend the three-dimensional world, but recognizing the existence of "multiple trees" instead, we must involve multiple relative timings when modeling structuralized causal effects.

Remark 3. *Counterfactuals* can be viewed as posterior distributions in $\mathbb{R}^O \cup \mathbb{R}^T$ given priors in $\mathbb{R}^O$.

The ability of causal models to address counterfactual queries is a key factor that underscores its importance Scholkopf (2021), such as "What would the effect be if the cause were different?". The separation of the cognitive temporal space enhances this capability by facilitating the interpretation of counterfactuals as distributions. In particular, given a "what if" scenario, we can conceptualize the prior conditions as features within $\mathbb{R}^O$. This allows us to view the collection of all subsequent possibilities as a distribution across $\mathbb{R}^O \cup \mathbb{R}^T$ that responds to conditional queries to address counterfactuals. This perspective might potentially offer valuable insights in fields like quantum computing.

2.2 Dynamical vs. Sequential Static

Observable distributions along a dimension can be broadly classified into *linear* and *nonlinear* categories. Within the temporal dimension, these correspond to ***static*** and ***dynamical*** temporal features, respectively, and can be represented by corresponding variables. Static features are typically linked to specific timestamps. For instance, consider the statement "rain leads to wet floors"; here "wet floors" represents a state that can be identified at a particular point in time. Therefore, it can be denoted as a static variable X_t with a specified timestamp t. In contrast, the expression "floors becoming progressively wetter" necessitates a representation that captures the temporal distribution, to account for changes over time, like $X^t = (X_1, \ldots, X_t)$. However, this raises the question: Is X^t a dynamical variable or a sequence of static variables?

The distinction between "static" and "dynamical" models in machine learning refers to whether time is a factor in the model's equations PGMadhavan (2016), a distinction typically made between "models" instead of "variables", which is reasonable since the significance of temporal distributions depends on the specific demands of models. Individually, a variable can only be characterized as being *able* to incorporate **t** as a computational dimension or *not*. For instance, "floors becoming progressively wetter" can be roughly described as "linearly increasing from 0% to 100% in 10 minutes", representing a sequential static feature, or it can be depicted by a 10-dimensional nonlinear distribution as dynamics, if finer granularity is required.

Determining whether a functional model $Y_{t+1} = f(X_t; \theta)$ is static or dynamical hinges on whether the changes from X_t to Y_{t+1} are confined to be linear, as represented by θ. Conventionally, θ and Y are often considered

together, with θ representing all potential static and dynamical changes in a hybrid Weinberger & Allen (2022), while the observational Y_{t+1} alone displays the resultant static outcome at a specific timestamp.

In the proposed *Relation-Oriented* paradigm, the relation θ exists independently to signify certain unobservable information within $\mathbb{R}^H$ without any explicit distributional representation. This allows for considering $\mathcal{Y}$ as an individual variable encompassing the temporal dimension, thus able to represent dynamically significant effects caused by $\mathcal{X}$.

Definition 4. *Dynamical Variable* vs. Sequential Static Variable.
A ***dynamical*** variable $\mathcal{X} = \langle X, \mathbf{t} \rangle \in \mathbb{R}^O$ allows for *computational freedom* over $\mathbf{t}$, while a *sequential* ***static*** variable $X^t \in \mathbb{R}^{O-1}$ assums i.i.d. across $\mathbf{t}$. Both of their instances manifest as observational sequences $x^t = (x_1, \ldots, x_t)$ in data, where the dynamical significance of $\mathcal{X}$ is model-dependent.

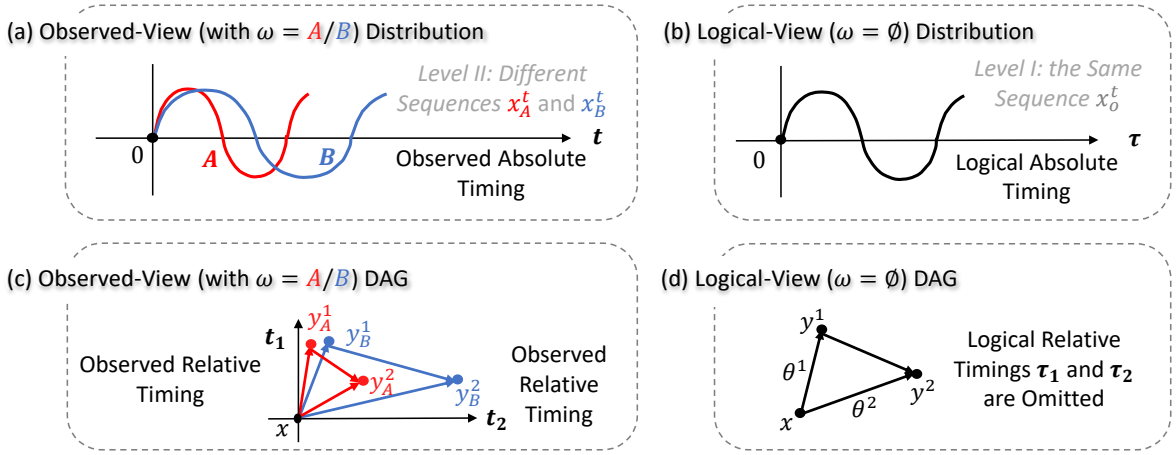

Figure 4: Comparisons of the individualized dynamics from the model's Observed-View, and the generalized ones from humans' Logical-View. (a) and (b) depict a unique distribution $\mathcal{X} \in \mathbb{R}^O$. (c) and (d) illustrate a structural relationship $\mathcal{X} \xrightarrow{\vartheta} \mathcal{Y}$ with $\mathcal{Y}$ comprising *confounded dynamics*, where $T = 2$ and $\vartheta = \overrightarrow{\theta^1 \theta^2}$.

$\mathcal{Y} = \langle Y, \tau \rangle$ enables the capture of nonlinear changes over time (such as varying progression speeds or so), making it dynamically significant per the models' demands. These effect dynamics may imply undetectable hierarchical levels due to the existence of ω, with each level encompassing the same timing dimensions, no matter for the absolute timing within observational $\mathbb{R}^O$, or the relative timings in cognitive $\mathbb{R}^T$.

When constructing knowledge, humans' cognition instinctively extracts general information ($\omega = \varnothing$) from various scenarios and, when applying this knowledge, individualizes it by adapting to specific scenarios (with varying ω values). Accordingly, it is unsurprising that the causal DAGs in our cognitive framework represent generalized knowledge only, and necessitate the generalizability of the causal models, to remain temporally multi-dimensional effective across the hierarchical levels. However, the undetectability of ω implies that models, whether they are AI-based neural networks or not, cannot autonomously fulfill such requirements.

Figure 4 uses two examples to showcase the different views from the models' and humans' perspectives, termed (individualized) Observed-View and (generalized) Logical-View, respectively. The causal DAG in (c) and (d) exhibits a typical *confounded dynamics* of the effect $\mathcal{Y}$, spanning two relative timings $\mathbf{t_1}$ and $\mathbf{t_2}$ in $\mathbb{R}^T$ with $T = 2$. The static instance values y_A^1 and y_B^1 indicate that the two individualized dynamical effects $\mathcal{Y}_A = (\mathcal{Y}_A^1, \mathcal{Y}_A^2)$ and $\mathcal{Y}_B = (\mathcal{Y}_B^1, \mathcal{Y}_B^2)$ attain an equivalent magnitude in $\mathbf{t_1}$ dimension, manifested as the same status valued y^1; and similarly on another timing dimension $\mathbf{t_2}$.

Remark 4. The generalization process of a structural causal relationship can be seen as a geometrically linear transformation process within the Observed-View DAG space.

2.3 Informative Hyper-Dimensional Space

Succinctly, the generalizable causal reasoning in our cognition can be represented by $(\vartheta, \omega) \in \mathbb{R}^T \cup \mathbb{R}^H$ across the hyper-dimensional and cognitive temporal spaces. Therefore, the causal reasoning AGI that we envisage can be defined as a system fully encompassing unobservable information denoted by (ϑ, ω), where $\vartheta \in \mathbb{R}^T \cup \mathbb{R}^H$ signifies a structural causal relationship over relative timings, and $\omega \in \mathbb{R}^H$ implies the capability of modeling nonlinearities in all dimensions, including temporal dynamics, to realize the generalizability of structural models across different levels of knowledge.

Figure 5 provides a fundamental overview of the prevailing methods in relationship modeling, corresponding to the limitations of the *Observation-Oriented* paradigm, as briefly summarized in Figure 1. In this context, we employ ϑ_ω to represent a hierarchical structural relationship and accordingly highlight two major obstacles we encounter. The first arises from the hidden relation ω (i.e., limitation L1), which limits the ability of the knowledge-driven Logical-View methods (like causal inference-based ones) to generalize models for Observed-View scenarios. The second relates to the cognitive relative timings foundational to our causal knowledge, encompassing structured dynamical effects; these timings are often overlooked by data-driven AI-based methods (i.e., limitation L2), impeding their capacity for causal reasoning.

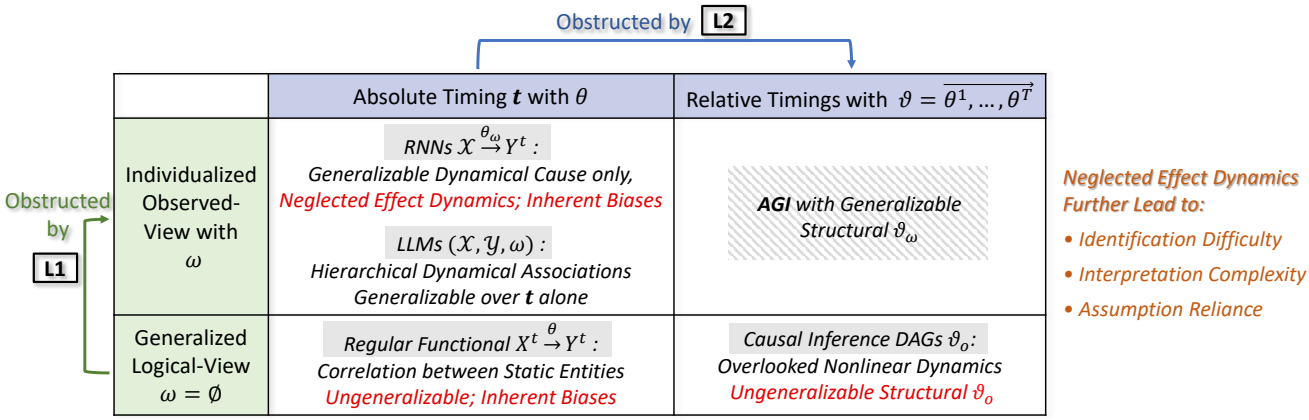

Figure 5: Detailed overview of major obstacles toward realizing AGI (referring to Figure 1 for L1 L2).

Regular functional models typically derive the parameter θ based on the correlation among static events with specified sequential timestamps. Notably, Granger causality Granger (1993), a method well-regarded in economics Maziarz (2015), introduces two separate temporal sequences for cause and effect, represented as X^t and Y^τ, seems to allow for multiple timings to a certain extent. However, the true significance lies in acknowledging the relative timings for their *nonlinear independence*, as this enables the representation of coexisting, varied temporal dynamics, particularly in the effects.

Remark 5. Distinguishing relative timings gains significance when the dynamics inherent in them are crucial for the model.

For models that do not account for temporal dimensional nonlinearities, identifying relative timings is not particularly significant. This is why traditional causal inference often omits explicit representation of relative timing axes in DAG structures, as shown in Figure 4 (d). While causal inference primarily adopts a *Relation-Oriented* perspective focused on structural knowledge, its failure to address nonlinearities can lead to a lack of dynamical generalizability when transforming Logical-View knowledge ϑ_o into practical Observed-View models within ϑ_ω. To address this, we suggest enhancing conventional causal DAGs to visually illustrate dynamical variations across multi-dimensional relative timings, a concept further detailed in Section 4.

Unsurprisingly, AI-based Recurrent Neural Network (RNN) models are increasingly favored in relationship modeling Xu et al. (2020), considering their proficiency in handling nonlinearities. RNNs, particularly, can transform observational sequence X^t into latent features, enabling the capture of nonlinearities across the

temporal dimension $\mathbf{t}$ to realize dynamical $\mathcal{X}$. However, while RNNs effectively address the dynamics within causes, they often overlook the potential dynamics of effects, resulting in a static representation of Y^t for $\mathcal{Y}$.

This *imbalance* in causal modeling is an essential flaw under the current *Observation-Oriented* paradigm, and accordingly motivated the emerging trend in *inverse learning* methods Arora (2021). The core reasons and wider implications of this neglect will be further explored in Section 3. Moreover, the overlooked structural ϑ may result in inherent biases, fundamentally undermining the identifiability of the dynamical entities in AI, forming a vital reason to reconsider the current paradigm, as detailed in Section 4.

On the other hand, the ability to extract the informative parameter θ distinguishes the anticipated knowledge comprehension by AGI from mere context-associative learning. Therefore, discussing structural knowledge ϑ within Large Language Models (LLMs) may still be premature.

In language learning tasks, the unobservable θ represents the semantic relation between phrases $\mathcal{X}$ and $\mathcal{Y}$, following only the absolute timing $\mathbf{t}$. Given the generally consistent sequential semantics of words, it is reasonable to dismiss the presence of relative timings. While LLMs may not explicitly extract θ, they can consistently reflect it by $(\mathcal{X}, \mathcal{Y})$. This phenomenon might help explain why AI can generate intelligent responses without truly "understanding" in the human sense, due to the lack of an extracted informative θ.

In solely observational learning tasks, such as image recognition, meta-learning is considered advantageous in deriving $\mathcal{I}(\omega)$ due to its inherent adaptability to different ω across various contexts Hospedales et al. (2021). Consequently, integrating meta-learning with LLMs could potentially enhance the hierarchical association $(\mathcal{X}, \mathcal{Y}, \omega)$, making it more generalizable over the $\mathbf{t}$ timing axis alone Lake (2023).

In essence, the current meta-learning remains confined to observational $(\mathcal{X}, \mathcal{Y})_\omega \in \mathbb{R}^O$, while an AGI system incorporating knowledge understanding should involve relational information represented by $\vartheta_\omega \in \mathbb{R}^T \cup \mathbb{R}^H$. It may stand to reason that the key to enabling AGI lies in implementing *Relation-Oriented* meta-learning.

3 Neglected Effect Dynamics in Causality

Traditional causal inference often highlights the interpretability of causal models, notably distinguishing them from mere correlations - Because these distinctions are not inherently embedded within the modeling context, but are mainly evident in model interpretations, potentially to guide improvements for the model. Given its statistical basis, the prevailing theories rooted in causal inference have not fully embraced the pivotal role of nonlinear temporal dynamics. This section concentrates on these often overlooked dynamics, aiming to provide a more intuitive understanding of causal learning.

Definition 5. Causality vs. Correlation in the modeling context.
- Causality $\mathcal{X} \xrightarrow{\vartheta} \mathcal{Y}$ is the relationship involving dynamically significant entities $\mathcal{X}$ and $\mathcal{Y}$.
- Correlation $X^t \xrightarrow{\theta} Y^t$ only includes static entities, possibly sequential static ones, X^t and Y^t.

In a modeling process, the causal directionality (i.e., the roles of cause and effect) may not impose restrictions, although it is often emphasized in model interpretations. Specifically, when selecting a model for a directional relationship $X \to Y$, one could use $Y = f(X; \theta)$ to predict the effect Y, or $X = g(Y; \phi)$ to inversely infer the cause X. Both parameters, θ and ϕ, are obtained from the joint probability $\mathbf{P}(X, Y)$ without imposing modeling constraints. We refer to it as *symmetric directionality* for clarity.

The empirical concerns for modeling directions mainly arise for two reasons: 1) to comply with our intuitive understanding of temporal progression; 2) the current causal modeling exhibits an ***imbalance*** in capturing dynamics between the cause and the effect - A typical example is the RNN models.

Timestamp t was introduced by the Picard-Lindelof theorem in the 1890s, initiating the functional form $Y_{t+1} = f(X_t)$ to represent time evolution. Then, time series learning methods, like the autoregressive model Hyvärinen (2010), facilitate the form of $Y_{t+m} = f(X^t)$ with a sequential causal variable X^t, where the time progress m from X to Y is predetermined. For RNNs, the latent space optimization over the representation of X^t is driven by predicting the observed Y_{t+m} through the parameterized relation θ. Consequently, the

significant temporal nonlinearity within X^t over $\mathbf{t}$ can be captured, enabling the form of $Y_{t+m} = f(\mathcal{X};\theta)$ with a dynamical cause $\mathcal{X}$. However, the effect Y_{t+m} remains static, leaving all potentially significant dynamics of the effect completely managed by the function f. Although f can be selected as linear or nonlinear to treat $\mathcal{X}$, the time evolution from t to $t+m$ is always left as ***linear***.

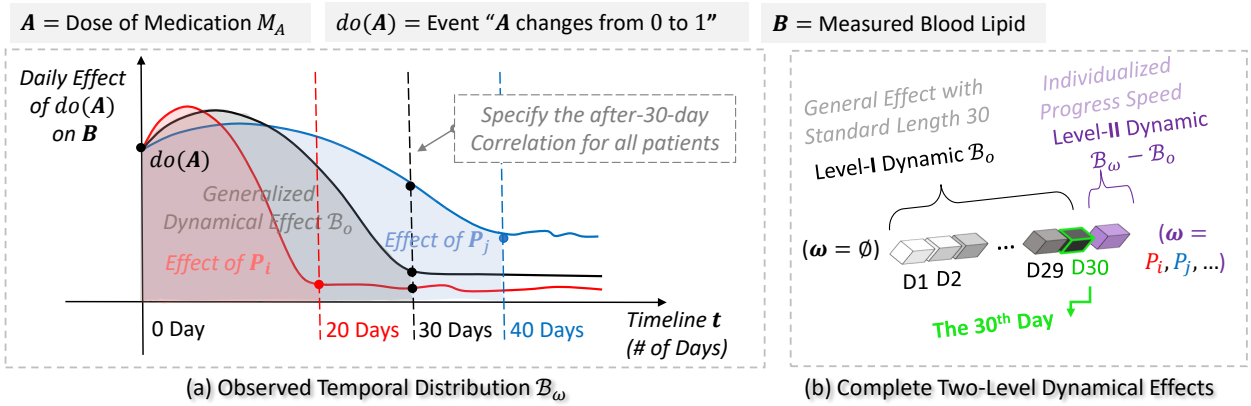

Figure 6: Medication M_A treats high blood lipid, with $do(A)$ denoting its initial use. It is given that the general-level effect $\mathcal{B}_o$ takes about 30 days to fully release ($t = 30$ at the elbow), depicted by the black curve in (a). Patient P_i achieves this effect curve elbow in 20 days, while patient P_j takes 40 days.

The example in Figure 6(a) illustrates the frequently incompletely captured dynamical effects in conventional causal models, where the action $do(A)$ causes the dynamical $\mathcal{B}_\omega$, observed as a sequence B^t. Two levels of dynamical features can be disentangled: **I** the generalized standard sequence of length 30, denoted by $\mathcal{B}_o$; **II** individualized progress variation $\mathcal{B}_\omega - \mathcal{B}_o$. For simplicity, assume the patients' unobserved personal characteristics uniformly accelerate or decelerate the effective progress, making $\omega = P_i, P_j, \ldots$ simply represent their speeds. The modeling objective is to obtain $\mathcal{B}_o$, as the effectiveness evaluation of M_A.

Conventionally, a clinical estimation is by averaging all patients' performances after 30 days, resulting in a correlation model $B_{t+30} = f(do(A_t))$, only capturing the final step B_{t+30} of $\mathcal{B}_o$ without the preceding 29 steps, as highlighted in (b). Yet, even with the adoption of a sequential variable B^t, such as in Granger causality, capturing $\mathcal{B}_o$ remains challenging, let alone the complete dynamic $\mathcal{B}_\omega$. Particularly, estimating B^t by averaging all patients' D1-D30 sequences requires the data to meet certain criteria: an exact 30-day span on average, the near-linear variations among patients, the near-normal variational distributions centered on D30, and others. In essence, this is to manually define the boundary of $\mathcal{B}_o$ by exploring all possible $\mathcal{B}_\omega$.

Hierarchical dynamical effects, prevalent in fields like epidemic progression, economic fluctuations, strategic decision-making, etc., often necessitate such manual examinations over potential values of ω to delineate the generalized-level features, such as group-specific learning methodologies Fuller et al. (2007). However, these traditional approaches are impractical in the context of large-scale relational learning within AI applications. Particularly in structural relationships, without manual specifications for each variable, their interchangeable roles of cause and effect can lead to amplified errors notable in the output.

3.1 Identification Difficulty of Dynamical Effects

In a relationship $\mathcal{X} \xrightarrow{\theta} \mathcal{Y}$, the *Observation-Oriented* paradigm typically requires specifying the sequential outcome $Y^t = (Y_1, \ldots, Y_t)$ to represent $\mathcal{Y}$. Then, a functional model $Y^t = f(\mathcal{X};\theta)$, usually based on existing knowledge, is employed to derive θ and subsequently produce a sequential estimate $\hat{Y}^t_\theta$ for Y^t with high accuracy. However, two types of errors present challenges: first, the discrepancy between the specified linear sequence and the targeted dynamical effect $\mid \mathcal{Y} - Y^t \mid$; second, the empirical modeling error from the predetermined θ. Together, these issues contribute to the difficulty of identifying dynamical effects in conventional causal modeling Zhang (2012).

Specifically, due to the static sequence Y^t, the task of representing neglected dynamics of $\mathcal{Y}$ shifts either to $f(;\theta)$ or to $\mathcal{X}$. In the former scenario, a factor σ representing "disturbance" is integrated into the function,

resulting in $f(;\theta+\sigma)$ Zhang (2012). In the latter case, as illustrated in do-calculus Pearl (2012); Huang (2012), the dynamics of $\mathcal{X}$ need to be manually discretized as identifiable temporal events to ensure their observational effects. This enables a fluid transformation from dynamical cause to observational effect, but the identifiability relies on non-experimental data (controllable θ) and can introduce additional complexities.

Considering the *differential* essence of do-calculus, we provide a streamlined reinterpretation of its three core rules from an *integral* viewpoint. Let $do(x_t) = (x_t, x_{t+1})$ indicate the occurrence of an instantaneous event $do(x)$ at time t, with the time step Δt sufficiently small to make the *interventional* effect of $do(x_t)$ identifiable as a function of the resultant distribution at $t+1$. Meanwhile, a separate *observational* effect is provoked by the static x_t. Then, the dynamical cause $\mathcal{X}$ can be discretized as below:

Given $\mathcal{X} \xrightarrow{\theta} Y$, where $\mathcal{X} = \langle X, t\rangle \in \mathbb{R}^{d+1}$ with the augmented $\mathbf{t}$ dimension residing a l-length sequence,

$$\mathcal{X} = \int_0^l do(x_t)\cdot x_t \; dt \quad \text{with} \quad \begin{cases} (do(x_t)=1) \mid \theta, & \textit{Observational} \text{ only (Rule 1)} \\ (x_t=1) \mid \theta, & \textit{Interventional} \text{ only (Rule 2)} \\ (do(x_t)=0) \mid \theta, & \text{No } \textit{interventional} \text{ (Rule 3)} \\ \text{otherwise} & \text{Associated } \textit{observational} \text{ and } \textit{interventional} \end{cases}$$

The effect of $\mathcal{X}$ can be derived as $f(\mathcal{X}) = \int_0^l f_t\big(do(x_t)\cdot x_t\big)\; dt = \sum_{t=0}^{l-1}(y_{t+1}-y_t) = y_L - y_0$

Given a controllable θ, it addresses three criteria that preserve conditional independence between *observational* and *interventional* effects, completing the chain rule, but sidesteps more generalized cases. When $\mathcal{Y} = \langle Y, \tau\rangle$ is defined as a dynamical effect, discretizing the dynamics in $do(y)$ remains necessary.

Another factor contributing to the identification issue is increased difficulty characterizing the effect sequence Y^t compared to the cause X^t. While organizing sequential data around a major causal event (e.g., days of heavy rain) is feasible, pinpointing the precise onset of subsequent effects (e.g., the exact day a flood began due to the rain) remains a more complex task. Moreover, in cases involving complex structural relations ϑ, overlooking relative timings may inherently impair the identifiability of Y^t, as detailed in Section 4.

Given the *symmetric directionality* nature of causal modeling, the inverse learning methodology Arora (2021) has recently garnered increasing attention, to achieve autonomous dynamical effect identification by inversely assigning the effect as the cause within RNNs. This approach capitalizes on the imbalance of RNNs in capturing dynamics between cause and effect, as represented by $Y = f(\mathcal{X};\theta)$. However, this inverse method does not address the structural ϑ, as the issue of impaired identifiability persists for X^t.

Remark 6. With a known relation θ from observables $\mathcal{X}$ to $\mathcal{Y}$, extracting the representation of $\mathcal{Y}$ by indexing through θ enables autonomous dynamical effect identification in the $\mathcal{X} \xrightarrow{\theta} \hat{\mathcal{Y}}_\theta$ relationship.

The *Relation-Oriented* modeling approach aims to derive θ between latent space representations of $\mathcal{X}$ and $\mathcal{Y}$, allowing for computational freedom in their temporal dimensions and enabling dynamical representations through optimization. Specifically, the initial sequences X^t and Y^t are transformed into a latent feature space $\mathbb{R}^L$. Within this $\mathbb{R}^L$ space, a neural network representing θ can be trained without prior assumptions (i.e., no required predetermination). This training progresses from cause to effect, formalizing sequentially associated representations $(\mathcal{X}, \theta, \hat{\mathcal{Y}}_\theta)$ and achieving relation-indexed optimization for both dynamical $\mathcal{X}$ and $\mathcal{Y}$ simultaneously. Detailed implementation will be outlined in Chapter II.

3.2 Interpretation Complexity

In traditional causal inference, the frequently neglected individual-level dynamics necessitate introducing the concept of a "hidden confounder", represented as node E in Figure 7 (a), which symbolizes unobserved personal characteristics in the scenario depicted in Figure 6. However, this approach does not necessarily require collecting additional data to identify E. This might lead to an illogical implication: "Our model is biased due to some unknown factors we don't intend to explore." Indeed, this strategy employs a solely observational causal variable, E, to account for the overlooked dynamical effect features. While E remains unknown, its inclusion can enhance model interpretation.

However, in the modeling context, as illustrated in Figure 7(b), the associative cause $do(A) * E$ remains unknown, failing to provide a modelable relationship for learning $\theta = (\theta_o, \theta_\omega)$. Consequently, this does not aid in enhancing the model's generalizability. In contrast, the *Relation-Oriented* approach does not necessitate additional modeling; it simply uses θ as indices to extract $\hat{\mathcal{Y}}_\theta$. This allows the utilization of any observed identifier linked to ω, like patient IDs, for instance. As depicted in (c), this knowledge-driven hierarchical disentanglement can effectively improve model generalizability.

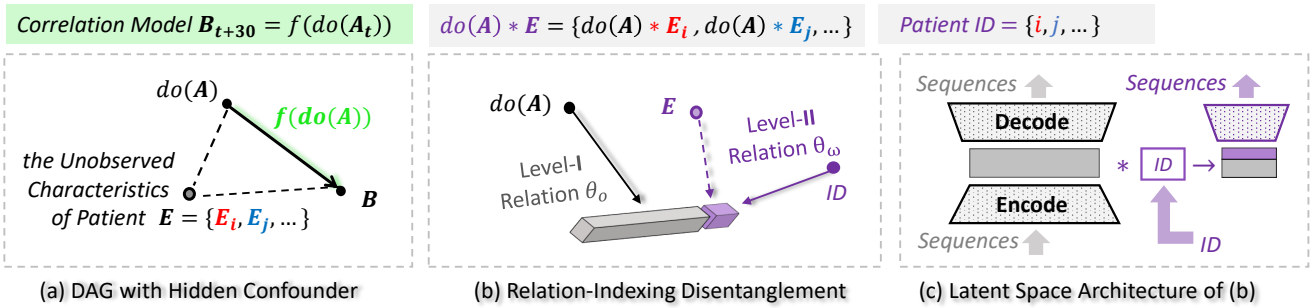

Figure 7: (a) Traditional causal inference DAG. (b) Hierarchical disentanglement of effect dynamics through relation-indexing. (c) Autoencoder-based generalized and individualized reconstruction processes.

3.3 Causal Assumptions Reliance

Due to the frequently overlooked effect dynamics, traditional causal learning typically relies on foundational causal assumptions to validate practical applications. In Figure 8, we categorize causal model applications into four distinct scenarios based on two aspects: Firstly, depending on whether the predetermination for θ is based on knowledge, they are divided into Causal Discovery and Causation Buildup. Secondly, they are further differentiated by the dynamical significance of their effects.

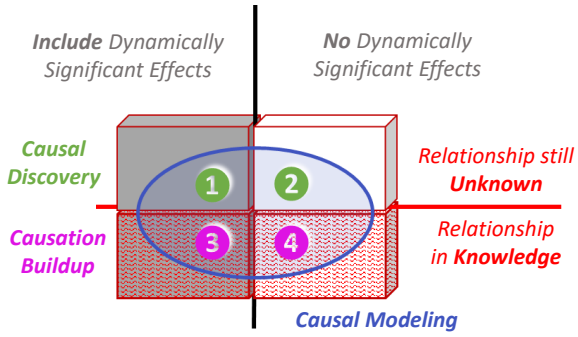

	Modeled Relation	***Modeled Directionality***
1	Observational Only. Undiscovered Dynamics covered by *Faithfulness Assumption.*	Observational Data Determined. Not Logically Meaningful.
2	Observational Only. Aligned with Knowledge.	Observational Data Determined. Maybe Logically Suggestive.
3	Knowledge Determined. Unmodeled Dynamics covered by *Hidden Confounders* or *Sufficiency Assumption.*	Knowledge Determined.
4	Knowledge Determined.	Knowledge Determined.

Figure 8: Categories of currently prevalent causal learning applications. The left rectangular cube illustrates causally meaningful relationships in logic, with the potentially modelable scope highlighted in blue.

As depicted in Figure 6 and Figure 7, the individual-level dynamics represented by θ_ω are often overlooked in the causal relation buildup process. Based on existing knowledge, some unobserved entities may be identified as hidden confounders, thereby enriching model interpretations. Nonetheless, if such identification is not easy, the foundational *Causal Sufficiency* assumption may lead to the complete neglect of these dynamics, presuming that all potential "hidden confounders" have been observed in the system.

On the other hand, causal discovery typically unearths structural relationships by detecting dependence among observables, but usually confined to their observational attributes excluding temporal features. If their dynamical features are not crucial, discovered associations can provide valuable insights into the underlying correlations; if they are essential, significant dynamics might be overlooked due to the *Causal Faithfulness* assumption, which suggests that captured observables can fully represent the causal reality.

Furthermore, although the discovered relationships are directional, these directions frequently lack a logical causal implication. Consider X and Y with predetermined directional models $Y = f(X;\theta)$ and $X = g(Y;\phi)$. The direction $X \to Y$ would be favored if $\mathcal{L}(\hat{\theta}) > \mathcal{L}(\hat{\phi})$. Let $\mathcal{I}_{X,Y}(\theta)$ denote the Fisher information about θ given $\mathbf{P}(X,Y)$. Use $p(\cdot)$ as the density function, and $\int_X p(x;\theta)dx$ remains constant in this context. Then:

$$\begin{aligned}\mathcal{I}_{X,Y}(\theta) &= \mathbb{E}[(\frac{\partial}{\partial\theta}\log p(X,Y;\theta))^2 \mid \theta] = \int_Y\int_X (\frac{\partial}{\partial\theta}\log p(x,y;\theta))^2 p(x,y;\theta)dxdy \\ &= \alpha\int_Y (\frac{\partial}{\partial\theta}\log p(y;x,\theta))^2 p(y;x,\theta)dy + \beta = \alpha\mathcal{I}_{Y|X}(\theta) + \beta, \text{with } \alpha,\beta \text{ being constants.}\end{aligned}$$

$$\text{Then, } \hat{\theta} = \arg\max_\theta \mathbf{P}(Y \mid X,\theta) = \arg\min_\theta \mathcal{I}_{Y|X}(\theta) = \arg\min_\theta \mathcal{I}_{X,Y}(\theta), \text{ and } \mathcal{L}(\hat{\theta}) \propto 1/\mathcal{I}_{X,Y}(\hat{\theta}).$$

The inferred directionality indicates how informatively the data reflects the two predetermined parameters, often representing mere statistical dependency. Consequently, such directionality is not logical but could be dominated by the data collection process, with the predominant entity deemed the "cause", consistent with some existing conclusions Reisach (2021); Kaiser (2021). Even when informative θ and ϕ are incorporated based on knowledge, they might not provide insights for dynamically significant causal relations.

4 Relative Timings in Structural Causality

Consider a structural relationship $\mathcal{Y} \xleftarrow{\theta_1} do(X) \xrightarrow{\theta_2} \mathcal{Z}$, where two dynamical effects of $do(X)$ progress along distinct relative timings $\mathbf{t_1}$ and $\mathbf{t_2}$. Initially, $\mathcal{Y}$ and $\mathcal{Z}$ are identified as sequences Y^t and Z^t according to absolute timing $\mathbf{t}$. If they are nonlinearly independent without interaction, denoted as $\theta_1 \perp \theta_2 \in \mathbb{R}^H$, then it may not be challenging for AI models like inverse RNNs to capture $\vartheta = \overrightarrow{\theta_1\theta_2}$ accurately, by utilizing the functional form $do(X) = f\big((Y,Z)^t;\vartheta\big)$ with associative identification $(Y,Z)^t = \big((Y,Z)_1,\ldots,(Y,Z)_t\big)$.

However, if $\mathcal{Y}$ and $\mathcal{Z}$ interact, like from $\mathcal{Y}$ to $\mathcal{Z}$, indicated by $Y \to Z$ for certain static values - which implies a dependence between $(\theta_1,\theta_2) \in \mathbb{R}^H$ in the hyper-dimensional space - then the associative identification $(Y,Z)^t$ could introduce ***inherent bias*** due to the ***confounded dynamics***, thereby reducing the model robustness and generalizability. Instead, it is necessary to initialize $Y^t = f_1(X)$ and $Z^t = f_2(X)$, and then engage in separate *relation-indexed learning* to obtain $\mathcal{Y} = f_1(X;\theta_1)$ and $\mathcal{Z} = f_2(X;\theta_2)$, respectively.

This section will first demonstrate the *inherent bias* through an intuitive example (section 4.1), explore its impact on the generalizability of structural causal models (section 4.2), and finally discuss the advancements and challenges on our path toward incorporating structural causal knowledge within AI (section 4.3).

4.1 Scheme of the Inherent Bias

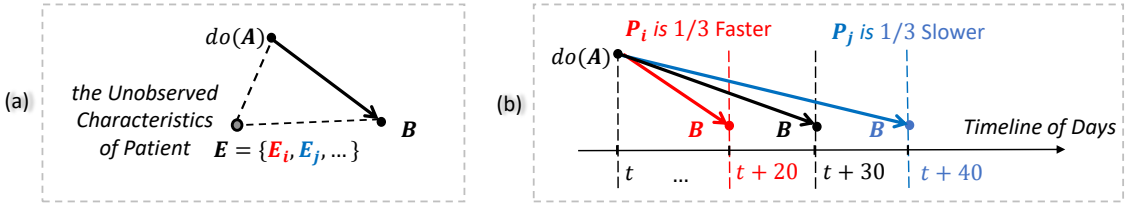

Figure 9: (a) Initial DAG introducing hidden E. (b) Enhanced DAG (Directed Acyclic Graph).

Consider Figure 9(a), which revisits the hidden-confounder inclusion depicted in Figure 6. To clearly represent the dynamical variations across multi-dimensional relative timings, we propose an enhancement to the conventional causal DAGs. This enhancement, as shown in (b), is carried out through two steps:

1. Consider dynamically significant effects and integrate their relative timings as individual dimensions.
2. Use varying edge lengths to signify the timespans required for reaching a certain effect magnitude, represented by a static value.

Figure 10(a) depicts a structural relationship $\mathcal{B} \xleftarrow{\theta_1} A \xrightarrow{\theta_2} \mathcal{C}$, extending from the scenario in Figure 9(b), with A succinctly replacing $do(A)$. It features two distinct effects: the primary effect $\mathcal{B}$ via θ_1, represented

by the edge $\overrightarrow{AB}$ leading to a static value for vital sign B; and a side effect $\mathcal{C}$ via θ_2 on another vital sign C, indicated by edge $\overrightarrow{AC}$. Notably, C can influence B, suggesting that A may also indirectly affect B through C, thereby creating *confounded dynamics* among the three entities across two timing axes $\mathbf{t_1}$ and $\mathbf{t_2}$.

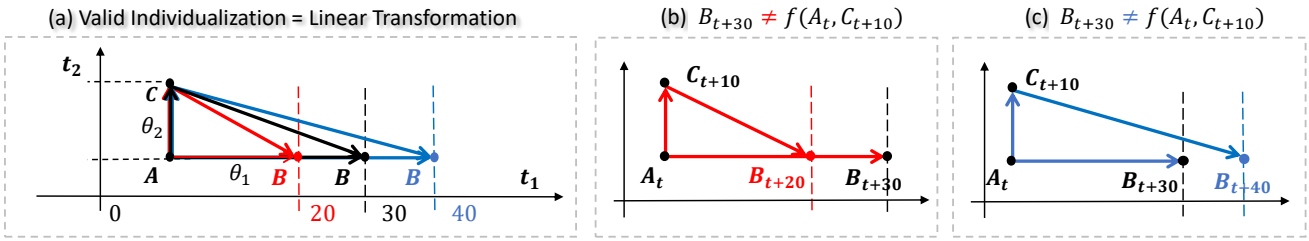

Figure 10: (a) The enhanced DAG with two relative timing axes. (b) (c) Violations of the Markov condition, when timestamps are specified for static effects identification, to construct SCMs.

For simplicity, we assume $\theta_1 \perp \theta_2 \in \mathbb{R}^H$, with the timespan of $\overrightarrow{AC}$ fixed at 10 days for all patients, and focus on modeling the static outcome B to predict the average fully-released medical effect in this population.

From a geometrical view, the triangle over nodes $\{A, B, C\}$ should remain closed across all populations and individuals to represent the same relationship, as supported by the *Causal Markov* condition. According to Remark 4, the generalization (and also individualization) process involves a linear transformation within the enhanced DAG space, depicted as "stretching" the triangle along $\mathbf{t_1}$ at various ratios, as in Figure 10(a).

In conventional Structural Causal Models (SCMs), the status of B is typically derived by setting an average timespan for the full release of medicine along $\overrightarrow{AB}$, say 30 days in this case. As illustrated in (b) and (c), the SCM function fails to shape a valid DAG for individual patients, represented by P_i in red and P_j in blue. Consequently, when extending to a sequential outcome like $B^t = (B_1, \ldots, B_{30})$, the B^t sequences for all patients would be treated as i.i.d. outcomes, implying sequential biases.

Definition 6. *Inherent Biases* that impair *Identifiabilities* of dynamical effects in SCM.
The *inherent bias* may occur in SCM if it contains: 1) *confounded dynamics* across *multiple* relative timings, and 2) undetectable hierarchy represented by ω.

In this simplified scenario, an inverse RNN model, formulated as $A = f\big((B, C)^t\big)$, could be effective due to the assumed independence. However, it is impractical to assume independence or the absence of confounded dynamics for all effects. This is particularly true in large models dealing with complex causal structures, where inherent biases can accumulate, ultimately jeopardizing the model's robustness.

4.2 Inherently Restricted Generalizability

To address the issues of *confounded dynamics*, traditional causal inference employs various methods to "de-confound"' them, such as cutting off interaction through propensity score matching Benedetto (2018) and backdoor adjustment Pearl (2009). However, these techniques often require specific tailoring for each application, necessitating manual identification of dynamically significant causal effects. Given the black-box nature and large scale of AI models, such manual adjustments have become increasingly impractical.

Moreover, these methods primarily focus on adapting to statistical linear models, which may not effectively contribute to dynamical generalizability. Subsequently, we will use a practical scenario to clearly illustrate how the specification of timestamps for effects inherently hinders the generalizability of the formulated SCMs.

Figure 11 displays an enhanced 3D view DAG, where Δt and $\Delta \tau$ signify actual time spans, particularly within the current population, to support the causal reasoning represented by this structure. Consider the triangle $SA'B'$: As each unit of effect from S delivered to A' (spent $\Delta\tau$), it immediately starts to impact B' through $\overrightarrow{A'B'}$ (Δt needed); meanwhile, the next unit begins generation at S. This dual action runs concurrently until S's effect fully reaches B', representing the single edge $\overrightarrow{SB'}$ within the SCM.

Due to the equation $\overrightarrow{SB'} = \overrightarrow{SA'} + \overrightarrow{A'B'}$, specifying the time span of $\overrightarrow{SB'}$ inherently determines the $\Delta t : \Delta\tau$ ratio based on the current population's performance, thereby fixing the shape of the ASB' triangle in the DAG space. If we focus solely on the accuracy of the estimated mean effect for this population, the SCM function $B' = f(A, C, S)$ can be effective. However, given that the preset $\Delta t : \Delta\tau$ ratio is not universally applicable, the generalizability of the established SCM to other populations becomes questionable.

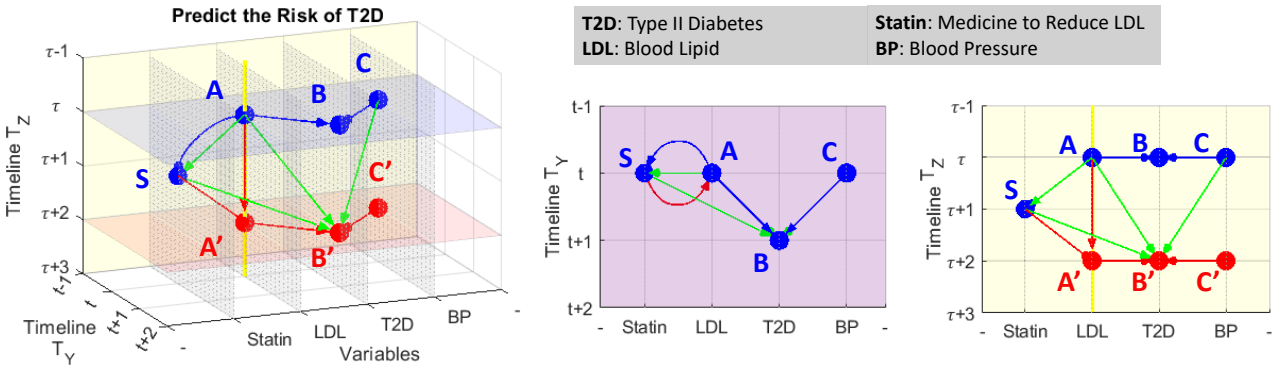

Figure 11: A DAG with two relative timing exes $\mathcal{T}_Y$ and $\mathcal{T}_Z$. The formulated SCM $B' = f(A, C, S)$ evaluates the effect of using S to reduce T2D risks at B'. On $\mathcal{T}_Y$, the step Δt from t to $(t+1)$ allows A and C to fully influence B. The step $\Delta\tau$ on $\mathcal{T}_Z$, from $(\tau+1)$ to $(\tau+2)$, let S fully release to forward status A to A'.

4.3 Developments Toward Causal Reasoning AI

In the pursuit of causal reasoning in machine learning, modeling techniques have evolved from capturing mere associations to learning observational correlations, ultimately advancing to structural causality modeling that incorporates the cognitive temporal space $\mathbb{R}^T$. Figure 12 summarizes this evolution in an upward trajectory.

Model	*Principle*	*Cause*	*Relation & Direction*	*Effect*	*Handle Undetectable Hierarchy*	*Capture Dynamics*
Mechanistic or Physical	$\mathcal{Y} = f(\mathcal{X}; \theta)$	Dynamical $\mathcal{X} = \langle X, \boldsymbol{t} \rangle$	by Knowledge	Dynamical $\mathcal{Y} = \langle Y, \boldsymbol{\tau} \rangle$	Yes	Yes
Relation-Indexing Approach	*Given* $\boldsymbol{P}(\mathcal{X}, \mathcal{Y})$ & $\mathcal{X} \overset{\vartheta}{\rightarrow} \mathcal{Y}$	Dynamical $\mathcal{X} = \langle X, \boldsymbol{t} \rangle$	by Representation $= f(\mathcal{X}, \vartheta, \hat{\mathcal{Y}}_\vartheta)$	Dynamical $\mathcal{Y} = \langle Y, \boldsymbol{\tau} \rangle$	Yes	Yes
Structural Causal Learning	*Given* $\boldsymbol{P}(X, Y)$ & $X \rightarrow Y$ $Y = f(X; \theta)$	Observational Sequence X^t	$X \rightarrow Y$ with Predetermined θ	Static Y_τ	?	?
Graphical Causal Discovery	*Given* $\boldsymbol{P}(X, Y)$ *Find* $\mathcal{L}(Y\|X; \theta) > \mathcal{L}(X\|Y; \theta)$	Observational X	Associated (X, Y) with insights into Correlation	Observational Y	?	No
Common Cause Model	*Given* $\boldsymbol{P}(X, Y\|Z)$	Observational X	Conditional Associated $(X, Y\|Z)$	Observational Y	?	No
i.i.d. Associative Model	*Given* $\boldsymbol{P}(X, Y)$	Observational X	None	Observational Y	No	No

Figure 12: Simple taxonomy of models (partially refer to Scholkopf (2021) Table 1), from more data-driven upward to more knowledge-driven. "?" means depending on the practice.

Given AI's ability to learn temporal dynamics, the current challenge is to deal with the dynamical interactions within $\mathbb{R}^O \cup \mathbb{R}^T$. However, as demonstrated in sections 4.1 and 4.2, even when modeling static outcomes, specifying timestamps to accomplish the required temporal events identification can still introduce inherent biases. Consequently, we need a knowledge-aligned manner to capture dynamics, specifically to align with our cognitive understanding, where the abstract relative timings underpin the causal knowledge's structures. This suggests a shift from the current *Observation-Oriented* paradigm towards a new one. Physical models, explicitly incorporated in temporal dimensional computation, may offer valuable insights into this prospect.

Under the observational i.i.d. assumption, initial models only approximate associations, proved unreliable for causal reasoning Pearl et al. (2000); Peters et al. (2017). Subsequently, the common cause principle highlights the significance of the nontrivial condition, to distinguish a relationship from statistical dependencies Dawid (1979); Geiger (1993), providing a basis for constructing graphical models Peters et al. (2014). The initial graphical model relies on conditional dependencies to construct Bayesian networks, with limited causal relevance Scheines (1997). Then, causally significance emphasizes the capability of addressing counterfactual queries Scholkopf (2021), like the structural equation models (SEMs) and functional causal models (FCMs) Glymour et al. (2019); Elwert (2013), which leverage prior knowledge to establish causal structures.

State-of-the-art deep learning on causality encodes the discrete, DAG-structural constraint into continuous optimization functions Zheng et al. (2018; 2020); Lachapelle et al. (2019), enabling advanced efficiency, but without noticeable generalizability, evident from the restricted successes in applications like the neural architecture search (NAS) Luo (2020); Ma (2018). This is reasonable, since the neglected relative timings can lead to inherent biases amplified through complex structures to become significant.

Scholkopf (2021) summarized our confronting key challenges toward generalizable causal-reasoning AI: 1) limited model robustness, 2) insufficient model reusability, and 3) inability to handle data heterogeneity (i.e., undetectable hierarchies). They are intrinsically linked to the demonstrated inherent biases.

Chapter II: Realization of Proposed Relation-Oriented Paradigm

This chapter introduces the proposed *Relation-Indexed Representation Learning* (RIRL) method, a baseline realization of the raised *Relation-Oriented* modeling paradigm. RIRL primarily focuses on autonomously identifying dynamical effects, in the form of relation-indexed representations in the latent space. In the context of structural modeling, RIRL enables hierarchical disentanglement of effects, according to given DAGs, as a manner of realizing dynamical generalizability across undetectable levels within knowledge. As a baseline realization, RIRL is suitable for applications with mature structural causal knowledge, and plenty of data to support neural network training on each known causal relationship.

First, Section 5 details the technique for extracting relation-indexed representations. Building on this, Section 6 presents the RIRL method of establishing structural causal models in the latent space. Lastly, Section 7 provides experiments to validate RIRL's efficacy in autonomously identifying effects.

5 Relation-Indexed Representation

In the relationship $\mathcal{X} \to \mathcal{Y}$, we define dynamical $\mathcal{X} = \langle X, t\rangle \in \mathbb{R}^{d+1} \subseteq \mathbb{R}^O$ and $\mathcal{Y} = \langle Y, \tau\rangle \in \mathbb{R}^{b+1} \subseteq \mathbb{R}^O$, given their solely observational variables, $X \in \mathbb{R}^d$ and $Y \in \mathbb{R}^b$. $\mathcal{X}$ is observed as a data sequence, represented by $X^t = (X_1, \ldots, X_t)$ with a pre-determined length l_x. For clarity, hereafter in this chapter, its instance x^t will be considered as a $(d{*}l_x)$-dimensional vector, denoted by $\overrightarrow{x}$ (or x for briefty). Similarly, $\mathcal{Y}$ is observed as the data sequence Y^t with a pre-determined length l_y, and its instance is referred to as a $(b{*}l_y)$-dimensional vector $\overrightarrow{y}$ (or y for briefty).

The relation-indexed representation aims to formulate $(\mathcal{X}, \theta, \hat{\mathcal{Y}}_\theta)$ in the latent space $\mathbb{R}^L$, beginning with an *initialization* to transform X^t and Y^t to be latent space features. For the sake of clarity, we use $\mathcal{H} \in \mathbb{R}^L$ and $\mathcal{V} \in \mathbb{R}^L$ to refer to the latent representations of $\mathcal{X} \in \mathbb{R}^O$ and $\mathcal{Y} \in \mathbb{R}^O$, respectively.

The modeling process is to optimize the neural network function $f(;\theta)$ in $\mathbb{R}^L$, with $\mathcal{H}$ as its input and $\mathcal{V}$ as the output. This process simultaneously refines $\mathcal{H}$, θ, and $\mathcal{V}$, for ultimately achieving $(\mathcal{H}, \theta, \hat{\mathcal{V}}_\theta) = (\mathcal{X}, \theta, \hat{\mathcal{Y}}_\theta)$. The refining will present as the distance minimization between $\mathcal{H}$ and $\mathcal{V}$ within $\mathbb{R}^L$. Consequently, the dimensionality L of the latent feature space must satisfy $L \geq rank(\mathcal{X}, \theta, \mathcal{Y})$, raising a technical challenge that L is larger than the dimensionality of $\overrightarrow{x}$ or $\overrightarrow{y}$.

Remark 7. The variable *initialization* necessitates a *higher-dimensional* representation autoencoder.

5.1 Higher-Dimensional Autoencoder

Autoencoders are commonly used for dimensionality reduction, especially in structural modeling that involves multiple variables Wang (2016). In contrast, RIRL aims to model individual causal relationships sequentially within a higher-dimensional latent space $\mathbb{R}^L$, as to hierarchically construct the entire causal structure. As illustrated in Figure 13, the designed autoencoder architecture is featured by the symmetrical *Expander* and *Reducer* layers (source code is available [1]). The Expander magnifies the input vector $\overrightarrow{x}$ by capturing its higher-order associative features, while the Reducer symmetrically diminishes dimensionality and reverts to its initial state. For precise reconstruction, the *invertibility* of these processes is essential.

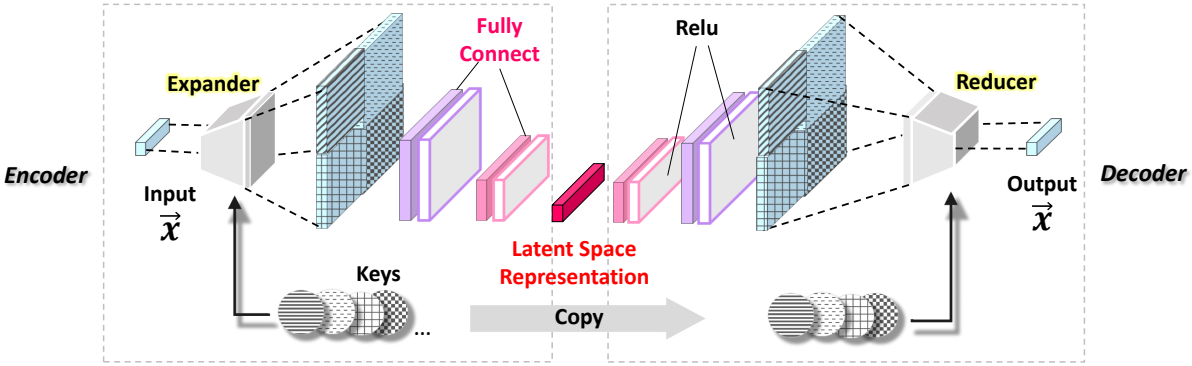

Figure 13: *Invertible* autoencoder architecture for extracting *higher-dimensional* representations.

The Expander showcased in Figure 13 implements a *double-wise* expansion. Here, every duo of digits from $\overrightarrow{x}$ is encoded into a new digit using an association with a random constant, termed the *Key*. This *Key* is generated by the encoder and replicated by the decoder. Such pairwise processing of $\overrightarrow{x}$ expands its length from $(d*l_x)$ to be $(d*l_x-1)^2$. By leveraging multiple *Keys* and concatenating their resultant vectors, $\overrightarrow{x}$ can be considerably expanded, ready for the subsequent dimensionality-reduced representation extraction. The four blue squares with unique grid patterns represent expansions by four distinct *Keys*, with the grid patterns acting as their "signatures". Each square symbolizes a $(d*l_x-1)^2$ length vector. Similarly, higher-order expansions, like *triple-wise* across three digits, can be achieved with adapted *Keys*.

Figure 14 illustrates the encoding and decoding processes within the Expander and Reducer, targeting the digit pair (x_i, x_j) for $i \neq j \in 1, \ldots, d$. The Expander function is defined as $\eta_\phi(x_i, x_j) = x_j \otimes exp(s(x_i)) + t(x_i)$, which hinges on two elementary functions, $s(\cdot)$ and $t(\cdot)$. The *Key* parameter, ϕ, embodies their weights, $\phi = (w_s, w_t)$. Specifically, the Expander morphs x_j into a new digit y_j utilizing x_i as a chosen attribute. In contrast, the Reducer symmetrically uses the inverse function η_ϕ^{-1}, defined as $(y_j - t(y_i)) \otimes exp(-s(y_i))$. This method avoids calculating s^{-1} or t^{-1}, granting flexibility for nonlinear transformations to $s(\cdot)$ and $t(\cdot)$. This design is inspired by the pioneering work of Dinh et al. (2016) on invertible neural network layers that utilize bijective functions.

5.2 Optimization Steps

Consider instances x and y of $\mathcal{X}$ and $\mathcal{Y}$, with corresponding representations h and v in $\mathbb{R}^L$. The latent dependency $\mathbf{P}(v|h)$ is used to train the relation function $f(;\theta)$, as illustrated in Figure 15. In each iteration, the modeling process undergoes three optimization steps:

1. Optimizing the cause-encoder by $\mathbf{P}(h|x)$, the relation model by $\mathbf{P}(v|h)$, and the effect-decoder by $\mathbf{P}(y|v)$ to reconstruct the relationship $x \to y$, represented as $h \to v$ in $\mathbb{R}^L$.
2. Fine-tuning the effect-encoder $\mathbf{P}(v|y)$ and effect-decoder $\mathbf{P}(y|v)$ to accurately represent y.
3. Fine-tuning the cause-encoder $\mathbf{P}(h|x)$ and cause-decoder $\mathbf{P}(x|h)$ to accurately represent x.

During this process, the values of h and v are iteratively adjusted to reduce their distance in $\mathbb{R}^L$, with $f(;\theta)$ serving as a bridge to span the distance. Here, the hyper-dimensional variable $\theta \in \mathbb{R}^H$ acts as the

[1] https://github.com/kflijia/bijective_crossing_functions/blob/main/code_bicross_extracter.py

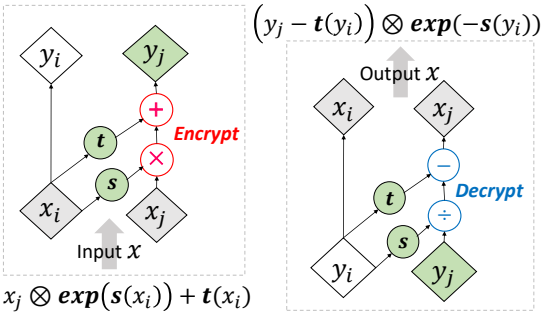

Figure 14: Expander (left) and Reducer (right).

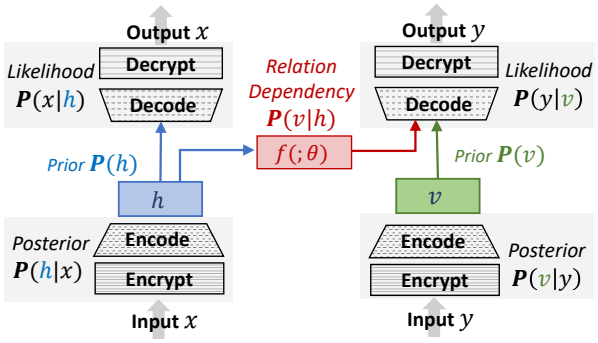

Figure 15: Relationship model architecture.

index, guiding the output of $f(;\theta)$ to encapsulate associated representations $(\mathcal{H}, \theta, \hat{\mathcal{V}}_\theta)$. From $\hat{\mathcal{V}}_\theta$, the effect component $\hat{\mathcal{Y}}_\theta$ can be reconstructed. Within the system, for each effect, a series of such relation functions $\{f(;\theta)\}$ is maintained, indexing diverse levels of causal inputs for sequentially building the structural model.

6 RIRL: Building Structural Models in Latent Space

By sequentially constructing relation-indexed representations for each pairwise relationship within the causal DAG, we can progressively achieve hierarchically disentangled representations for individual nodes. These representations align with the ω levels defined by the global structure, while simultaneously, the entire causal DAG structure will also be established accordingly. Subsequently, section 6.1 introduces the method for stacking higher-level representations upon established lower-level ones for individual effects. Section 6.2 then elaborates on the complete factorization process for hierarchical disentanglement. Finally, section 6.3 discusses a causal discovery algorithm within the latent space for initialized variable representations.

Figure 16 demonstrates how the RIRL method can encapsulate the black-box nature of AI within the latent space while simultaneously generating interpretable observations. This ability can be used to enhance existing *Observation-Oriented* models, for instance, by facilitating on-demand counterfactual simulations. Meanwhile, in the latent space, these cryptic representations, although opaque to human interpretation, play a crucial role in achieving model generalization and individualization. These processes are latently managed by AI and remain exclusive to human comprehension.

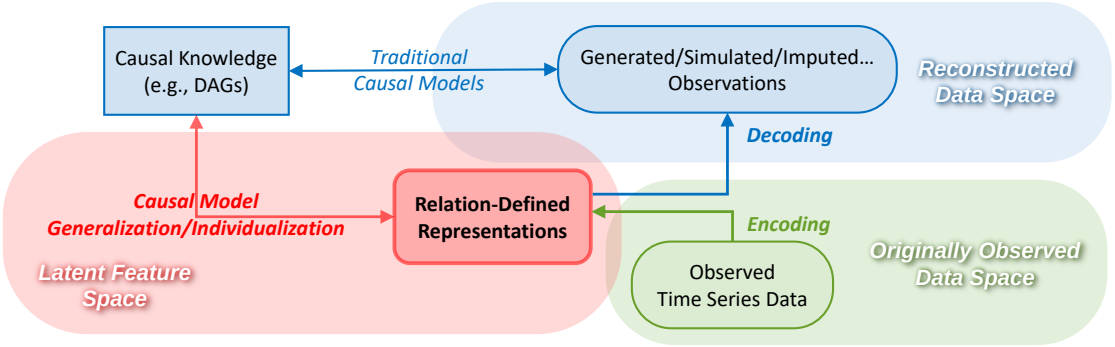

Figure 16: How Relation-Indexed Representation Learning (RIRL) contributes to traditional models.

6.1 Stacking Hierarchical Representations

A structural relationship can be represented by a causal graph, denoted as G. To construct models in the latent space, the latent dimensionality L must be sufficiently large to adequately represent G. Let's denote a data matrix augmented by all observational attributes in G as $\mathbf{X}$. Given the need to include informative relations $\{\theta\}$ for the edges in G, it is essential that $L > rank(\mathbf{X}) + T$, where T indicates the number of dynamically significant variables (i.e., nodes) within G.

The PCA principle posits that the space $\mathbb{R}^L$ learned by the autoencoder is spanned by the top principal components of $\mathbf{X}$ Baldi (1989); Plaut (2018); Wang (2016). Hypothetically, reducing L below $rank(\mathbf{X})$ may yield a less adequate but causally more significant latent space through better alignment of dimensions Jain (2021) (Further exploration in this direction is warranted). Bypassing a deep dive into dimensionality boundaries, we rely on empirical fine-tuning for the experiments in this study (reducing L from 64 to 16).

Consider a causal structural among $\{\mathcal{X}, \mathcal{Y}, \mathcal{Z}\}$, with their corresponding representations $\{\mathcal{H}, \mathcal{V}, \mathcal{K}\} \in \mathbb{R}^L$ initialized by three autoencoders, respectively. Figure 17 illustrates the hierarchical representations buildup. Here, two stacking scenarios are displayed based on varying causal directions. With the established $\mathcal{X} \to \mathcal{Y}$ relationship in $\mathbb{R}^L$, the left-side architecture finalizes the $\mathcal{X} \to \mathcal{Y} \leftarrow \mathcal{Z}$ structure, while the right-side focuses on $\mathcal{X} \to \mathcal{Y} \to \mathcal{Z}$. Through the addition of a representation layer, hierarchical disentanglement is formed, allowing for various input-output combinations (denoted as $\mapsto$) according to specific requirements.

For example, on the left, $\mathbf{P}(v|h) \mapsto \mathbf{P}(\alpha)$ represents the $\mathcal{X} \to \mathcal{Y}$ relationship, whereas $\mathbf{P}(\alpha|k)$ implies $\mathcal{Z} \to \mathcal{Y}$. Conversely, on the right, $\mathbf{P}(v) \mapsto P(\beta|k)$ denotes the $\mathcal{Y} \to \mathcal{Z}$ relationship with $\mathcal{Y}$ as input. Meanwhile, $\mathbf{P}(v|h) \mapsto P(\beta|k)$ captures the causal sequence $\mathcal{X} \to \mathcal{Y} \to \mathcal{Z}$.

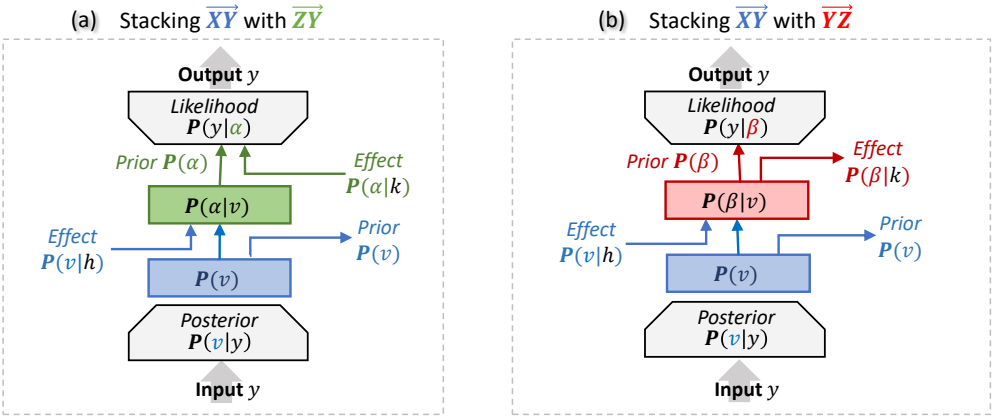

Figure 17: Stacking relation-indexed representations to construct hierarchy.

6.2 Factorizing the Effect Disentanglement

Consider $\mathcal{Y} = \langle X, \tau \rangle \in \mathbb{R}^{b+1} \subseteq \mathbb{R}^O$ having a T-level hierarchy, with each level built up using a representation function, labeled as g_t for the t-th level. For simplicity, here, we use ω_t to represent the t-th level component of $\mathcal{Y}$ in the latent space $\mathbb{R}^L$, while its counterpart in $\mathbb{R}^{b+1}$ is denoted as Ω_t. Let the feature vector ω_t in $\mathbb{R}^L$ primarily spans a sub-dimensional space, $\mathbb{R}^{L_t}$, resulting in the spatial disentanglement sequence $\{\mathbb{R}^{L_1}, \ldots, \mathbb{R}^{L_t}, \ldots, \mathbb{R}^{L_T}\}$, which hierarchically represents $\mathcal{Y}$ with T relative timings. Function g_t maps from $\mathbb{R}^{b+1}$ to $\mathbb{R}^{L_t}$, taking into account features from all previous levels as attributes. This gives us:

$$\mathcal{Y} = \sum_{t=1}^{n} \Omega_t, \text{ where } \Omega_t = g_t\big(\omega_t;\ \Omega_1, \ldots, \Omega_{t-1}\big) \text{ with } \Omega_t \in \mathbb{R}^{b+1} \text{ and } \omega_t \in \mathbb{R}^{L_t} \subseteq \mathbb{R}^L \tag{1}$$

In the context of a purely observational hierarchy, with $\mathcal{Y}$ substituted by $Y \in \mathbb{R}^b$, The example depicted in Figure 2 (b) can be interpreted as follows: Consider three feature levels represented as $\omega_1 \in \mathbb{R}^{L_1}$, $\omega_2 \in \mathbb{R}^{L_2}$, and $\omega_3 \in \mathbb{R}^{L_3}$. For simplicity, assume each subspace is mutually exclusive, such that $L = L_1 + L_2 + L_3$. In the latent space, the triplet $\langle \omega_1, \omega_2, \omega_3 \rangle \in \mathbb{R}^L$ comprehensively depicts the image. Their observable counterparts, Ω_1, Ω_2, and Ω_3, are three distinct full-scale images, each showcasing different content. For example, Ω_1 emphasizes finger details, while the combination $\Omega_1 + \Omega_2$ reveals the entire hand.

6.3 Causal Discovery in Latent Space

Algorithm 1 outlines the heuristic procedure for investigating edges among the initialized variable representations. We use Kullback-Leibler Divergence (KLD) as a metric to evaluate the strength of causal relationships.

Specifically, as depicted in Figure 15, KLD evaluates the similarity between the relation output $\mathbf{P}(v|h)$ and the prior $\mathbf{P}(v)$. Lower KLD values indicate stronger causal relationships due to closer alignment with the ground truth. Conversely, while Mean Squared Error (MSE) is a frequently used evaluation metric, its sensitivity to data variances Reisach (2021) leads us to utilize it as a supplementary measure in this study.

Algorithm 1: Latent Space Causal Discovery

Result: ordered edges set $\mathbf{E} = \{e_1, \ldots, e_n\}$
$\mathbf{E} = \{\}$; $N_R = \{n_0 \mid n_0 \in N, Parent(n_0) = \varnothing\}$;
while $N_R \subset N$ **do**
  $\Delta = \{\}$;
  for $n \in N$ **do**
    for $p \in Parent(n)$ **do**
      if $n \notin N_R$ *and* $p \in N_R$ **then**
        $e = (p, n)$; $\beta = \{\}$;
        for $r \in N_R$ **do**
          if $r \in Parent(n)$ *and* $r \neq p$ **then**
            $\beta = \beta \cup r$
          end
        end
        $\delta_e = K(\beta \cup p, n) - K(\beta, n)$;
        $\Delta = \Delta \cup \delta_e$;
      end
    end
  end
  $\sigma = argmin_e(\delta_e \mid \delta_e \in \Delta)$;
  $\mathbf{E} = \mathbf{E} \cup \sigma$; $N_R = N_R \cup n_\sigma$;
end

$G = (N, E)$	graph G consists of N and E
N	the set of nodes
E	the set of edges
N_R	the set of reachable nodes
$\mathbf{E}$	the list of discovered edges
$K(\beta, n)$	KLD metric of effect $\beta \to n$
β	the cause nodes
n	the effect node
δ_e	KLD Gain of candidate edge e
$\Delta = \{\delta_e\}$	the set $\{\delta_e\}$ for e
n,p,r	notations of nodes
e,σ	notations of edges

Figure 18 illustrates the causal structure discovery process in latent space over four steps. Two edges, (e_1 and e_3), are sequentially selected, with e_1 setting node B as the starting point for e_3. In step 3, edge e_2 from A to C is deselected and reassessed due to the new edge e_3 altering C's existing causal conditions. The final DAG represents the resulting causal structure.

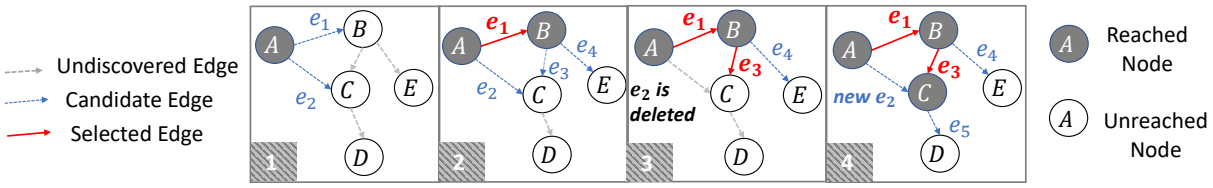

Figure 18: An example of causal discovery in the latent space.

7 Efficacy Validation Experiments

The experiments aim to validate the efficacy of the RIRL method from three aspects: 1) the performance of the proposed higher-dimensional representations, evaluated by reconstruction accuracy, 2) the construction of a clear effect hierarchy through the stacking of relation-indexed representations, and 3) the identification of DAG structures within the latent space through discovery. A full demonstration of the conducted experiments is available online [2]. The experiments in this study present two primary limitations, detailed as follows:

Firstly, the dataset used in the current experiments may not be optimal for assessing the efficacy of RIRL. In particular, real-world causal data, such as clinical records, often contain inherent biases. While empirical constraints limited our access to such data for this study, the synthetic data we utilized may not be ideal for validating the improved model robustness conferred by RIRL. For experiments that validate the presence of such inherent biases, readers are referred to prior research Li et al. (2020).

Secondly, the time windows designated for cause and effect, l_x and l_y, are consistently set at 10 and 1, respectively. This constraint arose from an initial oversight in the experimental design, wherein the pivotal

[2] https://github.com/kflijia/bijective_crossing_functions.git

role of *dynamics* was not fully recognized, leading to restrictions set by the RNN pattern. This limitation manifests when constructing causal sequences, such as in $\mathcal{X} \to \mathcal{Y} \to \mathcal{Z}$. While the model adeptly captures single-hop effects, it struggles with two-hop information due to the dynamics in $\mathcal{Y}$ being segmented into statics by the effect window $l_y = 1$, resulting in a loss of dynamic information. However, extending the length of l_y does not pose a significant technical challenge to future works.

7.1 Hydrology Dataset

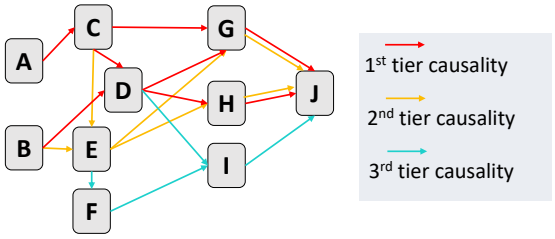

ID	Variable Name	Explanation
A	Environmental set I	Wind Speed, Humidity, Temperature
B	Environmental set II	Temperature, Solar Radiation, Precipitation
C	Evapotranspiration	Evaporation and transpiration
D	Snowpack	The winter frozen water in the ice form
E	Soil Water	Soil moisture in vadose zone
F	Aquifer	Groundwater storage
G	Surface Runoff	Flowing water over the land surface
H	Lateral	Vadose zone flow
I	Baseflow	Groundwater discharge
J	Streamflow	Sensors recorded outputs

Figure 19: Hydrological causal DAG: routine tiers organized by descending causal strength.

The dataset chosen for our experiments is a widely-used synthetic resource in the field of hydrology, aimed at enhancing streamflow predictions based on observed environmental conditions such as temperature and precipitation. In hydrology, deep learning, particularly RNN models, has gained favor for extracting observational representations and predicting streamflow Goodwell (2020); Kratzert (2018). We focus on a simulation of the Root River Headwater watershed in Southeast Minnesota, covering 60 consecutive virtual years with daily updates. The simulated data is from the Soil and Water Assessment Tool (SWAT), a comprehensive system grounded in physical modules, to generate dynamically significant hydrological time series.

Figure 19 displays the causal DAG employed by SWAT, complete with node descriptions. The hydrological routines are color-coded based on their contribution to output streamflow. Surface runoff (1st tier) significantly impacts rapid streamflow peaks, followed by lateral flow (2nd tier). Baseflow dynamics (3rd tier) have a subtler influence. Our causal discovery experiments aim to reveal these underlying tiers.

7.2 Higher-Dimensional Variable Representation Test

In this test, we have a total of ten variables (i.e., nodes), with each requiring an individual autoencoder for initialization. Table 1 lists the statistical characteristics of their post-scaled (i.e., normalized) attributes, along with their autoencoders' reconstruction accuracies. Accuracy is assessed in the root mean square error (RMSE), where a lower RMSE indicates higher accuracy for both scaled and unscaled data.

The task is challenging due to the limited dimensionalities of the ten variables - maxing out at just 5 and the target node, J, having just one attribute. To mitigate this, we duplicate the input vector to a consistent 12-length and add 12 dummy variables for months, resulting in a 24-dimensional input. A double-wise extension amplifies this to 576 dimensions, from which a 16-dimensional representation is extracted via the autoencoder. Another issue is the presence of meaningful zero-values, such as node D (Snowpack in winter), which contributes numerous zeros in other seasons and is closely linked to node E (Soil Water). We tackle this by adding non-zero indicator variables, called *masks*, evaluated via binary cross-entropy (BCE).

Despite challenges, RMSE values ranging from 0.01 to 0.09 indicate success, except for node F (the Aquifer). Given that aquifer research is still emerging (i.e., the 3rd tier baseflow routine), it is likely that node F in this synthetic dataset may better represent noise than meaningful data.

7.3 Hierarchical Disentanglement Test

Table 3 provides the performance comparison of stacking relation-indexed representations on each node. The term "single-effect" is to describe the accuracy of a specific effect node when reconstructed from a single cause

Table 1: Characteristics of node attributes and their variable representation test results.

Variable	Dim	Mean	Std	Min	Max	Non-Zero Rate%	RMSE on Scaled	RMSE on Unscaled	BCE of Mask
A	5	1.8513	1.5496	-3.3557	7.6809	87.54	0.093	0.871	0.095
B	4	0.7687	1.1353	-3.3557	5.9710	64.52	0.076	0.678	1.132
C	2	1.0342	1.0025	0.0	6.2145	94.42	0.037	0.089	0.428
D	3	0.0458	0.2005	0.0	5.2434	11.40	0.015	0.679	0.445
E	2	3.1449	1.0000	0.0285	5.0916	100	0.058	3.343	0.643
F	4	0.3922	0.8962	0.0	8.6122	59.08	0.326	7.178	2.045
G	4	0.7180	1.1064	0.0	8.2551	47.87	0.045	0.81	1.327
H	4	0.7344	1.0193	0.0	7.6350	49.93	0.045	0.009	1.345
I	3	0.1432	0.6137	0.0	8.3880	21.66	0.035	0.009	1.672
J	1	0.0410	0.2000	0.0	7.8903	21.75	0.007	0.098	1.088

Table 2: Brief summary of the latent space causal discovery test.

Edge	A→C	B→D	C→D	C→G	D→G	G→J	D→H	H→J	B→E	E→G	E→H	C→E	E→F	F→I	I→J	D→I
KLD	7.63	8.51	10.14	11.60	27.87	5.29	25.19	15.93	37.07	39.13	39.88	46.58	53.68	45.64	17.41	75.57
Gain	7.63	8.51	1.135	11.60	2.454	5.29	25.19	0.209	37.07	-5.91	-3.29	2.677	53.68	45.64	0.028	3.384

node (e.g., $B \to D$ and $C \to D$), and "full-effect" for the accuracy when all its cause nodes are stacked (e.g., $BC \to D$). To provide context, we also include baseline performance scores based on the initialized variable representations. During the relation learning process, the effect node serves two purposes: it maintains its own accurate representation (as per optimization no.2 in 5.2) and helps reconstruct the relationship (as per optimization no.1 in 5.2). Both aspects are evaluated in Table 3.

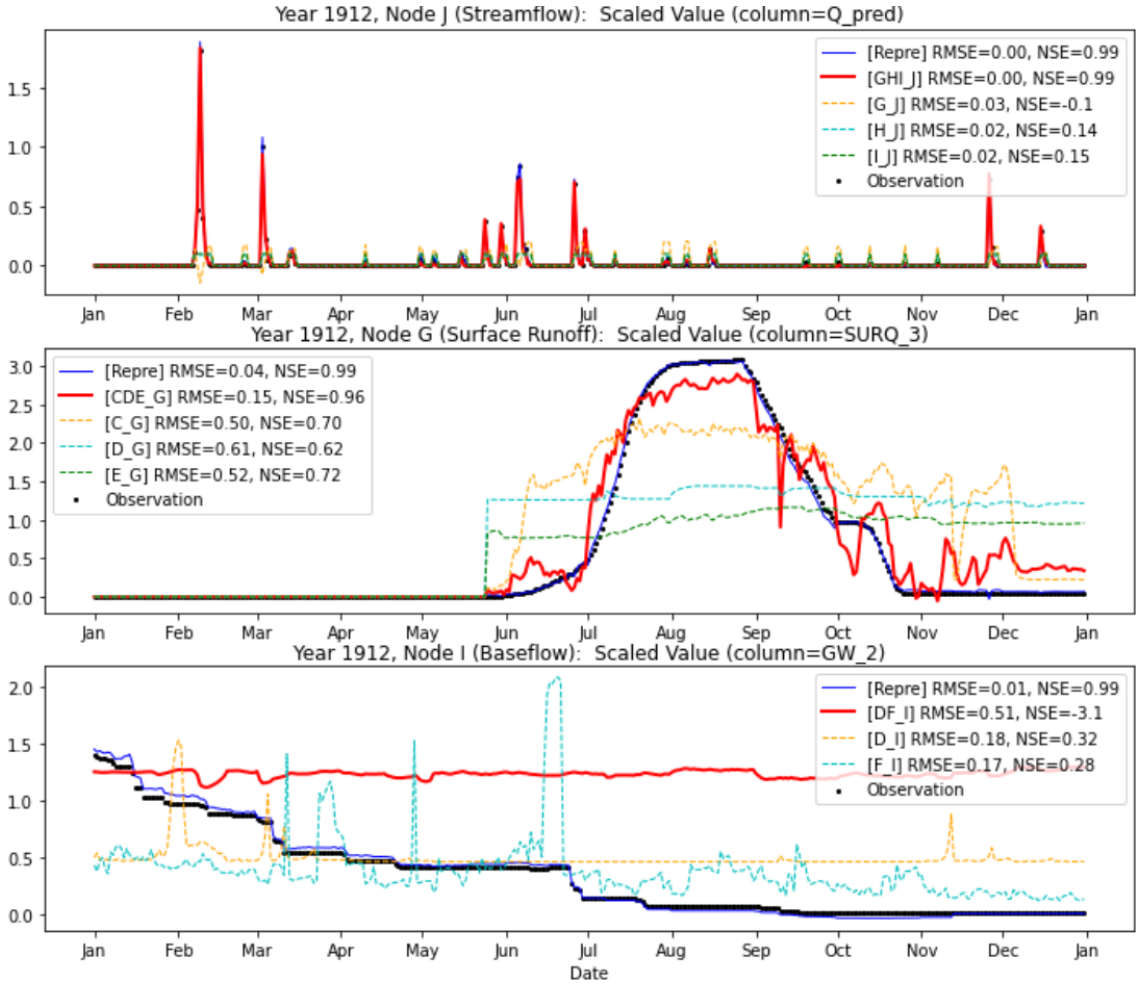

Figure 20: Reconstructed dynamical effects, via hierarchically stacked relation-indexed representations.

Table 3: Effect Reconstruction Performances of RIRL sorted by effect nodes.

Result Node	Variable Representation (Initial)			Cause Node	Variable Representation (in Relation Learning)			Relationship Reconstruction			
	RMSE		BCE		RMSE		BCE	RMSE		BCE	KLD
	on Scaled Values	on Unscaled Values	Mask		on Scaled Values	on Unscaled Values	Mask	on Scaled Values	on Unscaled Values	Mask	(in latent space)
C	0.037	0.089	0.428	A	0.0295	0.0616	0.4278	0.1747	0.3334	0.4278	7.6353
D	0.015	0.679	0.445	BC	0.0350	1.0179	0.1355	0.0509	1.7059	0.1285	9.6502
				B	0.0341	1.0361	0.1693	0.0516	1.7737	0.1925	8.5147
				C	0.0331	0.9818	0.3404	0.0512	1.7265	0.3667	10.149
E	0.058	3.343	0.643	BC	0.4612	26.605	0.6427	0.7827	45.149	0.6427	39.750
				B	0.6428	37.076	0.6427	0.8209	47.353	0.6427	37.072
				C	0.5212	30.065	1.2854	0.7939	45.791	1.2854	46.587
F	0.326	7.178	2.045	E	0.4334	8.3807	3.0895	0.4509	5.9553	3.0895	53.680
G	0.045	0.81	1.327	CDE	0.0538	0.9598	0.0878	0.1719	3.5736	0.1340	8.1360
				C	0.1057	1.4219	0.1078	0.2996	4.6278	0.1362	11.601
				D	0.1773	3.6083	0.1842	0.4112	8.0841	0.2228	27.879
				E	0.1949	4.7124	0.1482	0.5564	10.852	0.1877	39.133
H	0.045	0.009	1.345	DE	0.0889	0.0099	2.5980	0.3564	0.0096	2.5980	21.905
				D	0.0878	0.0104	0.0911	0.4301	0.0095	0.0911	25.198
				E	0.1162	0.0105	0.1482	0.5168	0.0097	3.8514	39.886
I	0.035	0.009	1.672	DF	0.0600	0.0103	3.4493	0.1158	0.0099	3.4493	49.033
				D	0.1212	0.0108	3.0048	0.2073	0.0108	3.0048	75.577
				F	0.0540	0.0102	3.4493	0.0948	0.0098	3.4493	45.648
J	0.007	0.098	1.088	GHI	0.0052	0.0742	0.2593	0.0090	0.1269	0.2937	5.5300
				G	0.0077	0.1085	0.4009	0.0099	0.1390	0.4375	5.2924
				H	0.0159	0.2239	0.4584	0.0393	0.5520	0.4938	15.930
				I	0.0308	0.4328	0.3818	0.0397	0.5564	0.3954	17.410

The KLD metrics in Table 3 indicate the strength of learned causality, with a lower value signifying stronger. For instance, node J's minimal KLD values suggest a significant effect caused by nodes G (Surface Runoff), H (Lateral), and I (Baseflow). In contrast, the high KLD values imply that predicting variable I using D and F is challenging. For nodes D, E, and J, the "full-effect" are moderate compared to their "single-effect" scores, suggesting a lack of informative associations among the cause nodes. In contrast, for nodes G and H, lower "full-effect" KLD values imply capturing meaningful associative effects through hierarchical stacking. The KLD metric also reveals the most contributive cause node to the effect node. For example, the proximity of the $C \rightarrow G$ strength to $CDE \rightarrow G$ suggests that C is the primary contributor to this causal relationship.

Figure 20 showcases reconstructed time series, for the effect nodes J, G, and I, in the same synthetic year to provide a straightforward overview of the hierarchical representation performances. Here, black dots represent the ground truth; the blue line indicates reconstruction via the initial variable representation, and the "full-effect" representation generates the red line. In addition to RMSE, we also employ the Nash–Sutcliffe model efficiency coefficient (NSE) as an accuracy metric, commonly used in hydrological predictions. The NSE ranges from -∞ to 1, with values closer to 1 indicating higher accuracy.

The initial variable representation closely aligns with the ground truth, as shown in Figure 20, attesting to the efficacy of our proposed autoencoder architecture. As expected, the "full-effect" performs better than the "single-effect" for each effect node. Node J exhibits the best prediction, whereas node I presents a challenge. For node G, causality from C proves to be significantly stronger than the other two, D and E.

7.4 Latent Space Causal Discovery Test

The discovery test initiates with source nodes A and B and proceeds to identify potential edges, culminating in the target node J. Candidate edges are selected based on their contributions to the overall KLD sum (less gain is better). Table 6 shows the order in which existing edges are discovered, along with the corresponding KLD sums and gains after each edge is included. Color-coding in the cells corresponds to Figure 19, indicating tiers of causal routines. The arrangement underscores the efficacy of this latent space discovery approach.

A comprehensive list of candidate edges evaluated in each discovery round is provided in Table 4 in Appendix A. For comparative purposes, we also performed a 10-fold cross-validation using the conventional FGES discovery method; those results are available in Table 5 in Appendix A.

8 Conclusions

In this paper, we propose a dimensionality framework, to symbolize and decompose our "cognitive space", where relational knowledge is stored. This framework offers a novel *Relation-Oriented* perspective, seeking to reevaluate the current relationship modeling paradigm. Specifically, conventional *Observation-Oriented* modeling, based on the i.i.d. assumption, intrinsically overlooks: the informative unobservables in $\mathbb{R}^H$, and the multi-dimensional dynamics in $\mathbb{R}^T$. Instead, it is confined to the observational space $\mathbb{R}^O$, relying on manually identifying dynamical effects from linearly observed sequences, inherently fraught with difficulty.

Viewed through the lens of the *Relation-Oriented* framework, multifaceted issues in causality learning become unified, encompassing common confusions and concerns, from traditional causal inference to modern LLMs. Recalling the queries outlined in the Introduction, we systematically summarize our current restrictions with new insights as follows:

- ❖ *Firstly*, challenges in causal inference primarily arise from overlooking effect dynamics, due to the linear modeling constraint. This oversight leads to compensatory efforts in various aspects, such as dealing with hidden confounders and relying on the causal sufficiency assumption. Causal DAGs naturally offer a *Relation-Oriented* view; with the proposed enhancement, they can provide fundamental support.
- ❖ *Secondly*, undetectable hierarchical levels, symbolized as the hidden relation $\omega \in \mathbb{R}^H$, are inherent in our knowledge. These levels drive the need for model generalizability. With AI's capability to capture dynamics, the main challenge is incorporating structural causal knowledge to achieve generalizable causal reasoning in AI. The current paradigm struggles with identifying dynamic effects, leading to inherent biases, while transitioning to knowledge-aligned modeling suggests a shift to the new paradigm.
- ❖ *Thirdly*, although existing language models, through meta-learning, have achieved more generalizable context associations, they remain limited to observational space bound to absolute timing, and are far from structuralized "comprehension" underpinned by relative timings in our cognitive framework. Nevertheless, LLMs have demonstrated the effectiveness of meta-learning across temporal dimensional hierarchies, indicating the potential of *Relation-Oriented* meta-learning in the pursuit of AGI.

We also raise a baseline implementation of the *Relation-Oriented* paradigm, with the primary purpose of verifying the effectiveness of the "relation-indexing" methodology in extracting causal representations on demand Scholkopf (2021). Indeed, in some domains with mature structural knowledge, effective attempts have emerged under similar principles, such as the introduction of hierarchical temporal memory in neuroscience Wu (2018). The journey to achieving AGI will undoubtedly be a historically extensive and complex undertaking, necessitating a vast array of knowledge-aligned AI model constructions. This study aspires to establish foundational insights for future developments in the field.

References

Daniel L Alkon, Howard Rasmussen. A spatial-temporal model of cell activation. *Science*, 239(4843):998–1005, 1988.

Natalia Andrienko, et al. Exploratory spatio-temporal visualization: an analytical review. *Journal of Visual Languages & Computing*, 14(6):503–541, 2003.

Saurabh Arora, Prashant Doshi. A survey of inverse reinforcement learning: Challenges, methods and progress. *Artificial Intelligence*, 297:103500, 2021.

Pierre Baldi, Kurt Hornik. Neural networks and principal component analysis: Learning from examples without local minima. *Neural networks*, 2(1):53–58, 1989.

Umberto Benedetto, et al. Statistical primer: propensity score matching and its alternatives. *European Journal of Cardio-Thoracic Surgery*, 53(6):1112–1117, 2018.

Seana Coulson, et al. Understanding timelines: Conceptual metaphor and conceptual integration. *Cognitive Semiotics*, 5(1-2):198–219, 2009.

William H Crown. Real-world evidence, causal inference, and machine learning. *Value in Health*, 22(5): 587–592, 2019.

A Philip Dawid. Conditional independence in statistical theory. *Journal of the Royal Statistical Society: Series B (Methodological)*, 41(1):1–15, 1979.

Laurent Dinh, Jascha Sohl, and Samy Bengio. Density estimation using real nvp. *arXiv:1605.08803*, 2016.

Felix Elwert. Graphical causal models. *Handbook of causal analysis for social research*, pp. 245–273, 2013.

Ursula Fuller, Colin G Johnson, Tuukka Ahoniemi, Diana Cukierman, Isidoro Hernán-Losada, Jana Jackova, Essi Lahtinen, Tracy L Lewis, Donna McGee Thompson, Charles Riedesel, et al. Developing a computer science-specific learning taxonomy. *ACm SIGCSE Bulletin*, 39(4):152–170, 2007.

Dan Geiger, et al. Logical and algorithmic properties of conditional independence and graphical models. *The annals of statistics*, 21(4):2001–2021, 1993.

Clark Glymour, Kun Zhang, and Peter Spirtes. Review of causal discovery methods based on graphical models. *Frontiers in genetics*, 10:524, 2019.

Allison E Goodwell, et al. Debates—does information theory provide a new paradigm for earth science? causality, interaction, and feedback. *Water Resources Research*, 56(2):e2019WR024940, 2020.

Clive WJ Granger, et al. Modelling non-linear economic relationships. *OUP Catalogue*, 1993.

Sander Greenland, et al. Confounding and collapsibility in causal inference. *Statistical science*, 14(1):29–46, 1999.

Timothy Hospedales, Antreas Antoniou, Paul Micaelli, and Amos Storkey. Meta-learning in neural networks: A survey. *IEEE transactions on pattern analysis and machine intelligence*, 44(9):5149–5169, 2021.

Yimin Huang, Marco Valtorta. Pearl's calculus of intervention is complete. *arXiv:1206.6831*, 2012.

Aapo Hyvärinen, et al. Estimation of a structural vector autoregression model using non-gaussianity. *Journal of Machine Learning Research*, 11(5), 2010.

Saachi Jain, et al. A mechanism for producing aligned latent spaces with autoencoders. *arXiv preprint arXiv:2106.15456*, 2021.

Marcus Kaiser, et al. Unsuitability of notears for causal graph discovery. *arXiv:2104.05441*, 2021.

Frederik Kratzert, et al. Rainfall–runoff modelling using lstm networks. *Hydrology and Earth System Sciences*, 22(11):6005–6022, 2018.

Sébastien Lachapelle, Philippe Brouillard, Tristan Deleu, and Simon Lacoste-Julien. Gradient-based neural dag learning. *arXiv preprint arXiv:1906.02226*, 2019.

Brenden M Lake, et al. Human-like systematic generalization through a meta-learning neural network. *Nature*, pp. 1–7, 2023.

Jia Li, Xiaowei Jia, Haoyu Yang, Vipin Kumar, Michael Steinbach, and Gyorgy Simon. Teaching deep learning causal effects improves predictive performance. *arXiv preprint arXiv:2011.05466*, 2020.

Yunan Luo, et al. When causal inference meets deep learning. *Nature Machine Intelligence*, 2(8):426–427, 2020.

Alexander Ly, Maarten Marsman, Josine Verhagen, Raoul PPP Grasman, and Eric-Jan Wagenmakers. A tutorial on fisher information. *Journal of Mathematical Psychology*, 80:40–55, 2017.

Jianzhu Ma, et al. Using deep learning to model the hierarchical structure and function of a cell. *Nature methods*, 15(4):290–298, 2018.

Gary Marcus. The next decade in ai: four steps towards robust artificial intelligence. *arXiv preprint arXiv:2002.06177*, 2020.

Tshilidzi Marwala. *Causality, correlation and artificial intelligence for rational decision making*. World Scientific, 2015.

Mariusz Maziarz. A review of the granger-causality fallacy. *The journal of philosophical economics: Reflections on economic and social issues*, 8(2):86–105, 2015.

Allen Newell, Herbert A Simon. Computer science as empirical inquiry: Symbols and search. In *ACM Turing award lectures*, pp. 1975. 2007.

Mohammed Ombadi, et al. Evaluation of methods for causal discovery in hydrometeorological systems. *Water Resources Research*, 56(7):e2020WR027251, 2020.

Ellie Pavlick. Symbols and grounding in large language models. *Philosophical Transactions of the Royal Society A*, 381(2251):20220041, 2023.

Judea Pearl. Causal inference in statistics: An overview. 2009.

Judea Pearl. The do-calculus revisited. *arXiv preprint arXiv:1210.4852*, 2012.

Judea Pearl et al. Models, reasoning and inference. *Cambridge, UK: CambridgeUniversityPress*, 19(2), 2000.

Jonas Peters, Joris M Mooij, Dominik Janzing, and Bernhard Schölkopf. Causal discovery with continuous additive noise models. 2014.

Jonas Peters, Dominik Janzing, and Bernhard Scholkopf. *Elements of causal inference: foundations and learning algorithms*. The MIT Press, 2017.

PGMadhavan. Static dynamical machine learning – what is the difference? `https://www.datasciencecentral.com/static-dynamical-machine-learning-what-is-the-difference/`, 2016.

David Pitt. Mental Representation. In Edward N. Zalta and Uri Nodelman (eds.), *The Stanford Encyclopedia of Philosophy*. Metaphysics Research Lab, Stanford University, Fall 2022 edition, 2022.

Elad Plaut. From principal subspaces to principal components with linear autoencoders. *arXiv:1804.10253*, 2018.

Alexander G Reisach, et al. Beware of the simulated dag! varsortability in additive noise models. *arXiv preprint arXiv:2102.13647*, 2021.

Schaeffer Rylan, et al. Are emergent abilities of large language models a mirage? *arXiv preprint arXiv:2304.15004*, 2023.

Pedro Sanchez, et al. Causal machine learning for healthcare and precision medicine. *Royal Society Open Science*, 9(8):220638, 2022.

Richard Scheines. An introduction to causal inference. 1997.

Bernhard Scholkopf, et al. Toward causal representation learning. *IEEE*, 109(5):612–634, 2021.

Charles H Shea, et al. Effects of an auditory model on the learning of relative and absolute timing. *Journal of motor behavior*, 33(2):127–138, 2001.

Michael E Sobel. An introduction to causal inference. *Sociological Methods & Research*, 24(3):353–379, 1996.

Richard S Sutton, Andrew G Barto. *Reinforcement learning: An introduction*. MIT press, 2018.

Monica G Turner. Spatial and temporal analysis of landscape patterns. *Landscape ecology*, 4:21–30, 1990.

Matej Vuković, Stefan Thalmann. Causal discovery in manufacturing: A structured literature review. *Journal of Manufacturing and Materials Processing*, 6(1):10, 2022.

Yasi Wang, et al. Auto-encoder based dimensionality reduction. 184:232–242, 2016.

Naftali Weinberger and Colin Allen. Static-dynamic hybridity in dynamical models of cognition. *Philosophy of Science*, 89(2):283–301, 2022.

Gurnee Wes, Tegmark Max. Language models represent space and time, 2023.

Christopher J Wood, Robert W Spekkens. The lesson of causal discovery algorithms for quantum correlations: Causal explanations of bell-inequality violations require fine-tuning. *New Journal of Physics*, 17(3):033002, 2015.

Jia Wu, et al. Hierarchical temporal memory method for time-series-based anomaly detection. *Neurocomputing*, 273:535–546, 2018.

Gabriele Wulf, et al. Reducing knowledge of results about relative versus absolute timing: Differential effects on learning. *Journal of motor behavior*, 26(4):362–369, 1994.

Haoyan Xu, Yida Huang, Ziheng Duan, Jie Feng, and Pengyu Song. Multivariate time series forecasting based on causal inference with transfer entropy and graph neural network. *arXiv:2005.01185*, 2020.

Kun Zhang, Aapo Hyvarinen. On the identifiability of the post-nonlinear causal model. *arXiv preprint arXiv:1205.2599*, 2012.

Xun Zheng, Bryon Aragam, Pradeep K Ravikumar, and Eric P Xing. Dags with no tears: Continuous optimization for structure learning. *Advances in neural information processing systems*, 31, 2018.

Xun Zheng, Chen Dan, Bryon Aragam, Pradeep Ravikumar, and Eric Xing. Learning sparse nonparametric dags. In *International Conference on Artificial Intelligence and Statistics*, pp. 3414–3425. PMLR, 2020.

A Appendix: Complete Experimental Results of Causal Discovery

Table 4: The Complete Results of Heuristic Causal Discovery in latent space. Each row stands for a round of detection, with '#" identifying the round number, and all candidate edges are listed with their KLD gains as below. 1) Green cells: the newly detected edges. 2) Red cells: the selected edge. 3) Blue cells: the trimmed edges accordingly.

# 1	**A→ C**	A→ D	A→ E	A→ F	**B→ C**	B→ D	B→ E	B→ F								
	7.6354	19.7407	60.1876	119.7730	**8.4753**	8.5147	65.9335	132.7717								
# 2	A→ D	A→ E	A→ F	B→ D	B→ E	B→ F	C→ D	C→ E	C→ F	C→ G	C→ H	C→ I				
	19.7407	60.1876	119.7730	**8.5147**	65.9335	132.7717	10.1490	46.5876	111.2978	11.6012	39.2361	95.1564				
# 3	**A→ D**	A→ E	A→ F	B→ E	B→ F	C→ D	C→ E	C→ F	C→ G	C→ H	C→ I	D→ E	D→ F	D→ G	D→ H	D→ I
	9.7357	60.1876	119.7730	65.9335	132.7717	**1.1355**	46.5876	111.2978	11.6012	39.2361	95.1564	63.7348	123.3203	27.8798	25.1988	75.5775
# 4	A→ E	A→ F	B→ E	B→ F	C→ E	C→ F	**C→ G**	C→ H	C→ I	D→ E	D→ F	D→ G	D→ H	D→ I		
	60.1876	119.7730	65.9335	132.7717	46.5876	111.2978	**11.6012**	39.2361	95.1564	63.7348	123.3203	27.8798	25.1988	75.5775		
# 5	A→ E	A→ F	B→ E	B→ F	C→ E	C→ F	C→ H	C→ I	D→ E	D→ F	D→ G	D→ H	D→ I	G→ J		
	60.1876	119.7730	65.9335	132.7717	46.5876	111.2978	39.2361	95.1564	63.7348	123.3203	**2.4540**	25.1988	75.5775	5.2924		
# 6	A→ E	A→ F	B→ E	B→ F	C→ E	C→ F	C→ H	C→ I	D→ E	D→ F	D→ H	D→ I	G→ J			
	60.1876	119.7730	65.9335	132.7717	46.5876	111.2978	39.2361	95.1564	63.7348	123.3203	25.1988	75.5775	**5.2924**			
# 7	A→ E	A→ F	B→ E	B→ F	C→ E	C→ F	**C→ H**	C→ I	D→ E	D→ F	D→ H	D→ I				
	60.1876	119.7730	65.9335	132.7717	46.5876	111.2978	**39.2361**	95.1564	63.7348	123.3203	**25.1988**	75.5775				
# 8	A→ E	A→ F	B→ E	B→ F	C→ E	C→ F	C→ I	D→ E	D→ F	D→ I	**H→ J**					
	60.1876	119.7730	65.9335	132.7717	46.5876	111.2978	95.1564	63.7348	123.3203	75.5775	**0.2092**					
# 9	**A→ E**	A→ F	B→ E	B→ F	**C→ E**	C→ F	C→ I	D→ E	D→ F	D→ I						
	60.1876	119.7730	65.9335	132.7717	**46.5876**	111.2978	95.1564	63.7348	123.3203	75.5775						
# 10	A→ F	B→ E	B→ F	C→ F	C→ I	**D→ E**	D→ F	D→ I	E→ F	E→ G	E→ H	E→ I				
	119.7730	**-6.8372**	132.7717	111.2978	95.1564	**17.0407**	123.3203	75.5775	53.6806	-5.9191	-3.2931	110.2558				
# 11	A→ F	B→ F	C→ F	C→ I	D→ F	D→ I	E→ F	**E→ G**	E→ H	E→ I						
	119.7730	132.7717	111.2978	95.1564	123.3203	75.5775	53.6806	**-5.9191**	-3.2931	110.2558						
# 12	A→ F	B→ F	C→ F	C→ I	D→ F	D→ I	E→ F	**E→ H**	E→ I							
	119.7730	132.7717	111.2978	95.1564	123.3203	75.5775	53.6806	**-3.2931**	110.2558							
# 13	**A→ F**	**B→ F**	**C→ F**	C→ I	**D→ F**	D→ I	**E→ F**	E→ I								
	119.7730	**132.7717**	**111.2978**	95.1564	**123.3203**	75.5775	**53.6806**	110.2558								
# 14	C→ I	D→ I	**E→ I**	**F→ I**												
	95.1564	75.5775	**110.2558**	**45.6490**												
# 15	C→ I	D→ I	**I→ J**													
	15.0222	3.3845	**0.0284**													
# 16	**C→ I**	**D→ I**														
	15.0222	**3.3845**														

Table 5: Average performance of 10-Fold FGES (Fast Greedy Equivalence Search) causal discovery, with the prior knowledge that each node can only cause the other nodes with the same or greater depth with it. An edge means connecting two attributes from two different nodes, respectively. Thus, the number of possible edges between two nodes is the multiplication of the numbers of their attributes, i.e., the lengths of their data vectors.
(All experiments are performed with 6 different Independent-Test kernels, including chi-square-test, d-sep-test, prob-test, disc-bic-test, fisher-z-test, mvplr-test. But their results turn out to be identical.)

Cause Node	A	B		C			D			E			F	G		H	I
True Causation	A→ C	B→ D	B→ E	C→ D	C→ E	C→ G	D→ G	D→ H	D→ I	E→ F	E→ G	E→ H	F→ I	G→ J		H→ J	I→ J
Number of Edges	16	24	16	6	4	8	12	12	9	8	8	8	12	4		4	3
Probability of Missing	0.038889	0.125	0.125	0.062	0.06875	0.039286	0.069048	0.2	0.142857	0.3	0.003571	0.2	0.142857	0.0		0.072727	0.030303
Wrong Causation Times of Wrongly Discovered				C→ F				D→ E	D→ F				F→ G	G→ H	G→ I	H→ I	
				5.6				1.2	0.8				5.0	8.2	3.0	2.8	

Table 6: Brief Results of the Heuristic Causal Discovery in latent space, identical with Table 3 in the paper body, for better comparison to the traditional FGES methods results on this page.
The edges are arranged in detected order (from left to right) and their measured causal strengths in each step are shown below correspondingly. Causal strength is measured by KLD values (less is stronger). Each round of detection is pursuing the least KLD gain globally. All evaluations are in 4-Fold validation average values. Different colors represent the ground truth causality strength tiers (referred to the Figure 10 in the paper body).

Causation	A→ C	B→ D	C→ D	C→ G	D→ G	G→ J	D→ H	H→ J	C→ E	B→ E	E→ G	E→ H	E→ F	F→ I	I→ J	D→ I
KLD	7.63	8.51	10.14	11.60	27.87	5.29	25.19	15.93	46.58	65.93	39.13	39.88	53.68	45.64	17.41	75.57
Gain	7.63	8.51	1.135	11.60	2.454	5.29	25.19	0.209	46.58	-6.84	-5.91	-3.29	53.68	45.64	0.028	3.384